

A mouse model for creatine transporter deficiency reveals early onset cognitive impairment and neuropathology associated with brain aging

Journal:	<i>Human Molecular Genetics</i>
Manuscript ID	HMG-2016-D-00593.R1
Manuscript Type:	2 General Article - UK Office
Date Submitted by the Author:	17-Jul-2016
Complete List of Authors:	<p>Baroncelli, Laura; CNR, Institute of Neuroscience Molinaro, Angelo; CNR, Institute of Neuroscience; University of Florence, Department of Neuroscience, Psychology, Drug Research and Child Health NEUROFARBA Cacciante, Francesco; Scuola Normale Superiore, BioSNS laboratory Alessandri, Maria Grazia; IRCCS Stella Maris Scientific Institute, Department of Developmental Neuroscience Napoli, Debora; Scuola Normale Superiore, BioSNS laboratory Putignano, Elena; CNR, Institute of Neuroscience Tola, Jonida; CNR, Institute of Neuroscience Leuzzi, Vincenzo; Sapienza University of Rome, Department of Paediatrics, Child Neurology and Psychiatry Cioni, Giovanni; IRCCS Stella Maris Scientific Institute, Department of Developmental Neuroscience; University of Pisa, Department of Clinical and Experimental Medicine Pizzorusso, Tommaso; CNR, Institute of Neuroscience; University of Florence, Department of Neuroscience, Psychology, Drug Research and Child Health NEUROFARBA</p>
Key Words:	creatine, aging, neurogenesis, neuroinflammation, oxidative stress

1
2
3 **A mouse model for creatine transporter deficiency reveals early onset cognitive impairment**
4 **and neuropathology associated with brain aging**
5
6
7
8
9

10 Laura Baroncelli^{1*}, Angelo Molinaro^{1,2}, Francesco Cacciante³, Maria Grazia Alessandri⁴, Debora
11 Napoli³, Elena Putignano¹, Jonida Tola¹, Vincenzo Leuzzi⁵, Giovanni Cioni^{4,6}, Tommaso
12 Pizzorusso^{1,2}
13
14
15

16
17
18 [1] Institute of Neuroscience, National Research Council (CNR), I-56124, Pisa, Italy
19

20
21 [2] Department of Neuroscience, Psychology, Drug Research and Child Health NEUROFARBA,
22 University of Florence, I-50135, Florence, Italy
23
24

25
26 [3] BioSNS laboratory, Scuola Normale Superiore di Pisa, I-56126, Pisa, Italy.
27
28

29
30 [4] Department of Developmental Neuroscience, IRCCS Stella Maris Scientific Institute, I-56018
31 IRCCS Stella Maris Foundation, I-56128Pisa, Italy
32
33

34
35 [5] Department of Paediatrics, Child Neurology and Psychiatry, Sapienza University of Rome, I-
36 00184, Rome, Italy
37
38

39
40 [6] Department of Clinical and Experimental Medicine, University of Pisa, I-56126, Pisa, Italy
41
42

43
44 Corresponding author:

45
46 Laura Baroncelli

47
48 Institute of Neuroscience, National Research Council (CNR) via Moruzzi

49
50 1, Pisa I-56124, Italy.

51
52 Email: baroncelli@in.cnr.it

53
54
55 Tel: +390 503 153199

56 Fax: +390 503 153220

57
58 **Abstract**
59
60

1
2
3 **Mutations in the creatine (Cr) transporter (CrT) gene lead to cerebral creatine deficiency**
4 **syndrome-1 (CCDS1), an X-linked metabolic disorder characterized by cerebral Cr deficiency**
5 **causing intellectual disability, seizures, movement and autistic-like behavioral disturbances,**
6 **language and speech impairment. Since no data are available about the neural and molecular**
7 **underpinnings of this disease, we performed a longitudinal analysis of behavioral and**
8 **pathological alterations associated with CrT deficiency in a CCDS1 mouse model. We found**
9 **precocious cognitive and autistic-like defects, mimicking the early key features of human**
10 **CCDS1. Moreover, mutant mice displayed a progressive impairment of short and long-term**
11 **declarative memory denoting an early brain aging. Pathological examination showed a**
12 **prominent loss of GABAergic synapses, marked activation of microglia, reduction of**
13 **hippocampal neurogenesis and accumulation of autofluorescent lipofuscin. Our data suggest**
14 **that brain Cr depletion causes both early intellectual disability and late progressive cognitive**
15 **decline, and identify novel targets to design intervention strategies aimed at overcoming brain**
16 **CCDS1 alterations.**
17
18
19
20
21
22
23
24
25
26
27
28
29
30
31
32
33
34
35
36
37
38
39
40
41
42
43
44
45
46
47
48
49
50
51
52
53
54
55
56
57
58
59
60

Introduction

Creatine (Cr) has a fundamental role in the energy metabolism of cells, particularly in tissues with high-energy demand. Cr kinase (CK) catalyzes the reversible conversion of Cr and ATP to phosphoCr (PCr) and ADP. Most of cells, indeed, do not rely on ATP/ADP free diffusion and the CK/PCr/Cr system serves as energy storage for immediate regeneration of ATP and as shuttle of high-energy phosphates between sites of ATP production and consumption (1). In physiological conditions, Cr is obtained by diet and by endogenous synthesis, which involves the enzymes L-arginine:glycineamidinotransferase (AGAT) and S-adenosyl-L-methionine:N-guanidinoacetatemethyltransferase (GAMT). Additionally, Cr is a polar hydrophilic molecule unable to cross the plasma membrane and a specific Na^+/Cl^- -dependent transporter (Cr transporter, CrT) is required for Cr to enter the cells (2).

The great relevance of Cr/PCr system for the normal functioning of brain cells is well supported by the recent discovery of three different pathologies characterized by defects of Cr metabolism that lead to primary neurological symptoms. AGAT (3) and GAMT disorders (4) are autosomal recessive conditions impairing Cr biosynthesis, while CrT deficiency (CCDS1) is an X-linked condition affecting cellular uptake of Cr (5). These disorders share the depletion of brain Cr and a similar clinical phenotype with intellectual disability, behavioral autistic-like abnormalities, language and speech disturbances, seizures and movement disorders (2, 6). Very little is known about Cr regulation and function in the brain. In the central nervous system, AGAT, GAMT and CrT are widely expressed in brain cells, including neurons, oligodendrocytes, and endothelial cells of the blood-brain barrier (7, 8). The lack of knowledge about the effects of Cr deficiency on neuronal circuits stems at least partially from the paucity of studies on animal models. Two germline murine models of CCDS1 and one model of GAMT deficiency are available so far (9–11), and they have been analyzed only in some behavioral domains and at neurochemical level, while studies on AGAT-deficient mice are limited to metabolic effects of Cr deficiency (12). Learning

1
2
3 and memory deficits, impaired motor activity and Cr depletion in brain and muscles have been
4 reported in GAMT and CrT models in the adult age (9–11). However, little is known about the
5 presence of autistic-like behavioral features and the onset and progression of the phenotype.
6
7

8
9
10 Several papers found that the disturbed energy metabolism caused by prolonged and
11 sustained Cr depletion might resonate in molecular networks resulting in abnormal metabolism.
12 Accordingly, the skeletal muscle of AGAT deficient mice display a marked increase of inorganic
13 phosphate/bATP ratio and overall mitochondrial content, while ATP levels were reduced by nearly
14 half (13). Patients with Cr deficiency syndrome are reported to have increased oxidative stress and
15 reactive oxygen species (ROS)-induced apoptotic cell loss (14), whereas Cr supplementation in
16 senescent mice improved neurobehavioral outcomes and prolonged median survival with a trend
17 towards lower ROS (15). We speculated that the disturbed energy metabolism caused by prolonged
18 and sustained Cr depletion might set in motion the precocious activation of detrimental cellular and
19 molecular mechanisms typical of brain aging leading to a progressive cognitive regression. The lack
20 of the antioxidant activity of Cr (16, 17) in CCDS1 might also contribute to this process (18). This
21 hypothesis would explain the observation that intellectual disability of CCDS1 patients seems to
22 become more pronounced with age (19). Intriguingly, our surmise could also be relevant for normal
23 brain aging as suggested by recent data showing that Cr levels are downregulated in aged human
24 brain (20, 21).
25
26
27
28
29
30
31
32
33
34
35
36
37
38
39
40
41
42

43 Thus, we performed a longitudinal evaluation of cognitive functions in CrT deficient mice
44 and we examined various age-related brain phenotypes including neuronal degeneration,
45 hippocampal neurogenesis, synaptic loss, neuroinflammation and oxidative stress. Our results show
46 that reduced Cr levels accelerate the brain aging process, indicating that CCDS1 could be
47 considered an age-dependent disorder and that alterations of Cr metabolism are directly involved in
48 brain aging.
49
50
51
52
53
54
55
56
57

58 **Results**

59
60

Reduced body weight growth in CrT^{-/-} mice

A first clue indicating that CrT deficiency elicits age-related detrimental effects emerged from the general appearance of mutant animals. Mice were weighed at different ages and compared with WT littermates. Even though no particular problems of breeding were observed and the face of CrT^{-/-} mice was normal till P40, CrT^{-/-} animals (n = 12) showed a significantly reduced body weight compared to CrT^{+/+} animals at P60, P100 and P180 (n = 13; Two way ANOVA on rank transformed data, p < 0.001 effect of genotype, p < 0.001 interaction between genotype and age; post hoc Holm Sidak method, p = 0.092 at P40, p < 0.001 in all other comparisons; Fig. S1).

Age-related deterioration of cognitive functions in Cr deficiency conditions

In previous behavioral investigation performed at P40, we highlighted that CrT^{-/-} mice exhibit a general cognitive impairment across different learning and memory tests (11). To understand whether a progressive deterioration of behavioral impairment is present in CrT^{-/-} mice, we studied four different stages: 1. during the early brain development (postnatal day (P) 28 at the beginning of testing), 2. during the late brain development (P40 at the beginning of testing), 3. in the adult age (P100 at the beginning of testing), and 4. in the middle age (P180 at the beginning of testing). Interestingly, a progressive worsening of cognitive symptoms was detectable in CrT^{-/-} mutant mice, suggesting that age is a key feature of Cr deficiency disease.

Y maze. We first analyzed the performance of CrT^{-/-} animals at P28 using the Y maze spontaneous alternation, which is an optimal task for probing memory in juveniles (Fig. 1a; (22)). Animals of both groups equally explored all the three arms of the maze. Indeed, no effect of genotype was detected for either the number of entries in the single arms of the maze (designated A, B, C) or the total number of arm entries, indicating that the exploratory disposition of mutant animals (n = 9) was not altered compared to WT littermates (n = 11; Two-Way ANOVA on rank transformed data, post hoc Holm-Sidak method, p = 0.506, p = 0.941, p = 0.276, p = 0.391 respectively, Fig. 1a). However, while in young WT mice alternation rate was about 60% of total arm choices, in CrT^{-/-}

1
2
3 animals it dropped to the chance level (50%; Fig. 1b), demonstrating that CrT disruption in the
4
5 mouse model could reproduce the early pathological phenotype of CCDS1 patients. The same
6
7 impairment was detected at P40, P100 and P180 with CrT^{-/-} mice performing at chance level
8
9 whereas WT age-matched controls showed significant spontaneous alternation (t test, p < 0.01 for
10
11 P40, p < 0.05 for P100 and P180, Fig. S2). These data also indicated that the spontaneous
12
13 alternation paradigm cannot reveal age-dependent cognitive decline in CrT mutants because of the
14
15 ceiling effect in the arm alternation deficit masking the effect of the age variable.
16
17

18 **Object recognition test (ORT).** We assessed declarative memory abilities in the ORT, a test based
19
20 on the spontaneous tendency of rodents to spend more time exploring a novel object than a familiar
21
22 one. No difference in short-term recognition memory between P40 CrT^{-/-} mice (n = 9) and age-
23
24 matched WT animals (n = 7) could be detected (t-test, p = 0.285). In contrast, the discrimination
25
26 index at 24 h was significantly lower in mutant mice, indicating that their capacity to recall the
27
28 familiar object was impaired (t-test, p < 0.05; Fig. 2a). This memory deficit became more
29
30 pronounced two months later (CrT^{-/-} n = 11, CrT^{+/+} n = 10; P100, t-test, p < 0.01 at 24h; Fig. 2b),
31
32 and eventually affecting both short and long-term memories at P180. Indeed, at P180 CrT^{-/-} mice
33
34 showed a marked memory deficit both at 1- and 24-h interval between the sample and the test phase
35
36 with respect to CrT^{+/+} mice (CrT^{-/-} n = 10, CrT^{+/+} n = 9; t-test, p < 0.05 for both comparisons; Fig.
37
38 2c), indicating that the longer the time during which neural circuits are forced to work without Cr
39
40 energy buffer the worse the cognitive performance of CrT^{-/-} animals.
41
42
43
44

45 **Morris water maze (MWM).** We further assessed memory abilities in the MWM, a cognitive
46
47 paradigm that allows testing spatial learning and memory. The probe test highlighted a spatial
48
49 memory impairment in Cr deficient mice at all the different ages tested: WT animals, indeed, spent
50
51 significantly longer time in the quadrant where the platform was located during the training days
52
53 (NE*; Two-Way RM ANOVA, post hoc Holm-Sidak method, p < 0.05 for all comparisons), while
54
55 mutant mice did not remember the location of the hidden platform and equally explored the four
56
57 quadrants of the maze (Two-Way RM ANOVA, post hoc Holm-Sidak method; Fig. S3).
58
59
60

1
2
3 The results obtained in the training phase of the MWM test, however, showed a clear
4 progression of cognitive deficits in CrT^{-y} mice. Since a main effect of genotype was found on mean
5 swimming speed recorded all along the training phase at the different ages tested (t-test, $p < 0.05$
6 (P40); Mann-Whitney Rank Sum test, $p < 0.05$ (P100); t-test, $p < 0.01$ (P180); Fig. S4), we
7 analyzed the length of path covered to find the submerged platform. At P40 CrT^{-y} animals ($n = 12$)
8 were able to learn the task as well as their age-matched WT controls ($n = 10$): although the mean
9 distance to locate the submerged platform on the last three days of training was longer in mutant
10 mice compared to CrT^{+y} littermates (t test, $p < 0.05$), they exhibited a progressive reduction of the
11 path length similar to WT littermates (Two-Way RM ANOVA, $p = 0.084$ effect of genotype) with a
12 significant difference between the two groups only at the day 5 of training (post hoc Holm-Sidak
13 method, $p < 0.05$; Fig. 3a). The same was true in P100 animals (CrT^{-y}: $n = 8$, CrT^{+y}: $n = 7$; Two-
14 Way RM ANOVA on rank transformed data, $p = 0.132$ effect of genotype, post hoc Holm-Sidak
15 method, $p < 0.05$ at day 5; Fig. 3b). In contrast, CrT^{-y} mice ($n = 7$) were significantly slower
16 learners with respect to age-matched WT mice ($n = 9$) at P180 so much so that the distance to locate
17 the platform was different between the two groups at days 3, 4, 5 and 6 of training (Two-Way RM
18 ANOVA on rank transformed data, genotype, $p < 0.001$, interaction between genotype and day $p <$
19 0.001 ; post hoc Holm-Sidak method, $p < 0.05$ for day 3 and 6, $p < 0.01$ for day 4 and 5; Fig. 3c).

20
21
22 To further corroborate the hypothesis of a premature cognitive decline in CrT null mice, we
23 compared the performance in the MWM of P180 CrT^{-y} animals and one-year old wild-type mice (n
24 $= 4$). The mean distance to locate the platform on the last three days of training (t-test, $p = 0.968$;
25 Fig. S5a) and the probe test revealed a similar learning and memory impairment in these two
26 experimental groups (Two-Way RM ANOVA, $p = 0.479$; Fig. S5b).

27 28 29 Emotional phenotype is not altered in CrT mutant animals

30
31
32 To rule out the possibility that significant differences in cognitive capacities reflect changes in the
33 ability to cope with stress in challenging task conditions, we analyzed general activity and anxiety-

1
2
3 related behavior of CrT^{-/-} and CrT^{+/-} mice in the open field arena at the different ages used for
4 cognitive assessment. We found that the time spent by CrT^{-/-} mutant mice (n = 12 for P40 and
5 P100, n = 11 for P180) in both the central and peripheral portion of the apparatus was not different
6 from that recorded for WT animals (n = 13 for P40 and P100, n = 11 for P180) at any of the time
7 point tested (Two Way ANOVA, post hoc Holm-Sidak method, p = 0.725 (P40), p = 0.508 (P100)
8 and p = 0.348 (P180)), indicating that the vulnerability to stress and anxiety responses are not
9 sensitive to CrT deletion and excluding the hypothesis that the progression of cognitive deficit
10 might be related to altered emotionality (Fig. S6).
11
12
13
14
15
16
17
18
19
20
21
22

23 **CrT^{-/-} mice exhibit increased repetitive and stereotyped behavior**

24 Since the clinical picture of CCDS1 patients include multiple traits linked to autism spectrum
25 disorders (ASDs), we also examined social behavior in CrT null mice. Although we used two
26 different social interaction paradigms, we detected no abnormalities in CrT^{-/-} mice at P180. In the
27 social preference test, indeed, both CrT^{-/-} (n = 8) and CrT^{+/-} (n = 6) animals spent significantly
28 more time exploring the wire cup housing the conspecific subject (Mann-Whitney Rank Sum test, p
29 = 0.662; Fig. 4a). Similarly, the discrimination index measured in the social novelty task did not
30 differ between mutant and WT mice (t-test, p = 0.784; Fig. 4a).
31
32
33
34
35
36
37
38
39
40

41 The second core ASD symptom domain includes repetitive and stereotyped movements,
42 routines, and rituals (23) and several mouse lines with ASD-associated mutations exhibit enhanced
43 learning on the accelerating rotarod, a task that requires formation and consolidation of a repetitive
44 motor routine (24). Thus, we tested rotarod abilities of CrT^{-/-} (n = 12 for P40, n = 11 for P100 and n
45 = 9 for P180) and CrT^{+/-} (n = 13 for P40 and P100, n = 11 for P180) animals, with the speed of
46 rotation accelerating from 4 to 40 rpm over 600 s. The performance of CrT^{-/-} mutant mice diverged
47 from that of wild-type mice, with a significant increase of fall latency from the drum at all ages
48 tested (Two Way ANOVA, effect of genotype p < 0.001, post hoc Holm Sidak method, p < 0.01 at
49 P40 and P100, p < 0.05 at P180; Fig. 4b). We next examined self-grooming, another stereotyped
50
51
52
53
54
55
56
57
58
59
60

1
2
3 behavior in mice (25). While no difference was present at P40 ($CrT^{-/y}$, n = 9; $CrT^{+/y}$, n = 7; Two
4
5 Way ANOVA on rank transformed data, post hoc Holm Sidak method, p = 0.912) CrT null mice
6
7 spent about threefold as much time grooming themselves as littermate WT mice at P180 ($CrT^{-/y}$, n
8
9 = 7; $CrT^{+/y}$, n = 11; p < 0.01; Fig. 4c).

14 **CrT deletion leads to a widespread Cr reduction in young and adult mice**

15
16 To understand whether the progression of cognitive deficits in $CrT^{-/y}$ mice was due to a gradual
17
18 reduction of brain Cr content, we measured Cr levels in various tissues in 1-month- and 6-month-
19
20 old animals using GC/MS. At both ages, we observed a significant reduction of Cr in the brain
21
22 (both cerebral cortex and hippocampus; Two Way ANOVA on rank transformed data, post hoc
23
24 Holm-Sidak method, p < 0.001), muscle (p < 0.001), heart (p < 0.001) and kidney (p < 0.05) of
25
26 $CrT^{-/y}$ mice with respect to wild-type (WT) littermates (n = 4/tissue for each group; Table 1).

27
28 Importantly, no difference was detected in Cr levels measured in the different tissues between P30
29
30 and P180 $CrT^{-/y}$ mice, except for the muscle: a Three way ANOVA on rank transformed data
31
32 analysis revealed a significant interaction (p < 0.001) between genotype and age only at level of
33
34 muscular tissue with a significant reduction of Cr levels in P180 $CrT^{-/y}$ mice (post hoc Holm-Sidak
35
36 method, p < 0.001). A moderate change in GAA levels was observed in some tissues (Table 2)
37
38 suggesting that Cr deficiency leads to a compensatory attempt by upregulating Cr biosynthesis.

39
40 Also in this case GAA content measured in P180 animals reproduced the levels reported in younger
41
42 tissues: a Three way ANOVA on rank transformed data revealed a significant interaction (p <
43
44 0.001) between genotype and age only at level of muscular tissue, but this analysis only stressed a
45
46 significant reduction of GAA levels in P180 $CrT^{-/y}$ (post hoc Holm-Sidak method, p < 0.05) and
47
48 WT mice (p < 0.001). These results allow rejecting the hypothesis that higher GAA toxicity could
49
50 underlie the age-related decline of cognitive functions in $CrT^{-/y}$ animals.
51
52
53
54
55
56
57
58

59 **Morphological characterization of neural circuits in $CrT^{-/y}$ mice**

1
2
3 The morpho-functional organization of neural circuits in mice carrying CrT mutations has never
4 been studied so far. Thus, we have investigated whether the accelerated decline of learning and
5 memory functions in CrT-deficient mice was accompanied by pathological changes in brain
6 morphology. The cerebral cortex and the hippocampus were analyzed because they are strictly
7 involved with the symptoms caused by CrT deficiency in mice and in humans. In the same animals
8 subjected to behavioral characterization, we first evaluated the neuroanatomical architecture of
9 prefrontal (PFC) and cingulate cortex (ACC) of P180 mice (n = 6 for both groups). Cortical
10 thickness and neuronal cell density was estimated on NeuN stained sections. No difference in the
11 cortical thickness (t-test, p = 0.785 for PFC and p = 0.880 for ACC; Fig. S6) and neuronal density
12 across cortical layers was observed in mutant animals (Two Way ANOVA, p = 0.683 for PFC;
13 Two Way ANOVA on rank transformed data, p = 0.146 for ACC; Fig. S7).

30 **Loss of GABAergic synapses in the cerebral cortex of CrT^{-/-} mice**

31 Since synaptic dysfunction is a feature commonly observed in normal aging and neurodegenerative
32 disorders likely contributing to pathology progression (26), we analyzed the synaptic punctate
33 expression of vGlut1 and vGAT, respectively as synaptic markers of excitatory and inhibitory
34 neurons, in the cerebral cortex of CrT^{-/-} mice. While excitatory synapses were not affected by Cr
35 deficiency (n = 6 for both groups; Mann-Whitney Rank Sum test, p = 0.792 for PFC; t-test, p =
36 0.340 for ACC; Fig. 5a), we detected a prominent loss of vGAT staining both in PFC and ACC,
37 suggesting a specific contribution of GABAergic synaptic alterations to the neuropathological
38 phenotype of CCDS1 (n = 9 for CrT^{-/-} group, n = 8 CrT^{+/+} group; t-test, p < 0.05 for both
39 comparisons; Fig. 5b). Importantly, the loss of vGAT-positive synapses overspread all the cortical
40 layers. These results are also consistent with previous studies on CCDS1 patients exhibiting
41 evidence for an epileptic phenotype (27) that could be predictive of a dysfunction of inhibitory
42 interneurons.

Microglial cell dysregulation in the Cr deficient brain

Since aberrant microglia activation is one of the main pathological hallmarks of brain aging (28, 29), we have also evaluated Iba-1 expression as a marker of possible morphological changes of microglia in the cerebral cortex (PFC) and the hippocampus (HP) of mutant mice. During aging microglia cells undergo morphological changes towards a reactive phenotype with short, thickened and less ramified processes (30). We found a strong increase of activated microglial cells in the brain of CrT null animals as compared to wild-type controls (n = 8 for both groups), with a parallel reduction of resting cells (Two Way ANOVA, post hoc Holm Sidak method, $p < 0.01$ for PFC and $p < 0.05$ for HP; Fig. 6a,b), indicating that the metabolic deficit caused by Cr deficiency leads to a dysfunction of brain-immune cells interactions and to a neuroinflammatory state that can contribute to the cognitive decline reported in CrT^{-/-} mice.

Reduced neurogenesis and enhanced lipofuscin accumulation in the hippocampus of CrT^{-/-} mice

It is well-known that the rate of neurogenesis declines dramatically with age and dysregulation of hippocampal neurogenesis is an important mechanism underlying the cognitive impairment associated with normal aging (31). In order to investigate whether CrT deficiency could affect hippocampal structure and impinge on the neurogenesis process, we examined neuronal proliferation through Ki67 labelling in the dentate gyrus (DG) of wild type and CrT^{-/-} mice (n = 6 for both groups). Stereological analysis first revealed that the hippocampal volume of mutant animals was markedly reduced with respect to that measured in control mice (t-test, $p < 0.05$; Fig. 7a). Accordingly, the number of Ki67-positive cell was significantly lower in the DG of CrT^{-/-} animal at P180, with approximately 30% reduction (t-test, $p < 0.01$; Fig. 7b,d). We also evaluated the number of immature neurons in hippocampal DG using the neuroblast marker doublecortin (DCX). DCX-positive cells were also significantly reduced in CrT null mice DG (t-test, $p < 0.001$;

1
2
3 Fig. 7c,e), demonstrating the impairment of adult hippocampal neurogenesis and suggesting another
4
5 cellular substrate of the cognitive deficit present in the CrT null model.
6

7
8 Another characteristic neuropathological finding in CrT mice was the massive accumulation
9
10 of autofluorescent material (lipofuscin). Lipofuscin is a lipopigment consisting of aggregated
11
12 products of lysosomal degradation, including oxidized and misfolded proteins, lipids, defective
13
14 mitochondria and metal ions (32). We observed a marked accumulation of autofluorescent
15
16 lipofuscin throughout the brain, but the most prominent autofluorescent signal was seen in the DG
17
18 hippocampal region. Lipofuscin deposition and accumulation within the hippocampal neurons is a
19
20 marker of cellular senescence (33); (34). Thus, we compared the area of lipofuscin granules in the
21
22 brain cells of 6-month-old CrT^{-/-} (n = 6) mice and their CrT^{+/+} siblings (n = 5). The accumulation of
23
24 lipofuscin was significantly exacerbated in the hippocampal DG of CrT^{-/-} animals at P180 (t-test, p
25
26 < 0.05, Fig. 7f,g).
27
28
29
30
31

32 **A conditional brain-specific model of CCDS1 recapitulates the phenotype displayed by CrT^{-/-}** 33 **mice**

34
35
36 Since CrT^{-/-} mice with ubiquitous deletion of the CrT gene showed a marked Cr depletion also in
37
38 peripheral tissues, we analyzed a novel mouse model in which a conditional CrT allele was deleted
39
40 in postmitotic neurons, glial cells and BBB endothelial cells by using the Nestin promoter to drive
41
42 Cre-recombinase expression (35; nes-CrT mice).
43
44

45
46 As expected, biochemical analysis in these mice highlighted a depletion of Cr (and a parallel
47
48 increase of GAA), similar to that of the null CrT mouse, totally restricted to
49
50 the brain tissue, with peripheral tissues being not affected (Table 3, 4). Importantly, we also
51
52 observed that CrT^{fl/y} animals not expressing Cre recombinase did not present a hypomorph
53
54 phenotype, with normal levels of Cr in different tissues (Table 3, 4). Behavioral investigation
55
56 highlighted that mutant (nes-CrT^{-/-}) animals showed an impaired performance in the object
57
58 recognition test (Fig. 8a) and a lower alternation rate in the Y maze (Fig. 8b), demonstrating an
59
60

1
2
3 impairment of both declarative and working memory reminiscent of the deficit described in the
4
5 ubiquitous model. More specifically, at P180 nes-CrT^{-/-} mice displayed an impaired discrimination
6
7 index with respect to nes-CrT^{+/-} mice both at 1- and 24-h interval between the sample and the test
8
9 phase (nes-CrT^{-/-} n = 6, nes-CrT^{+/-} n = 8; t-test, p < 0.05 for both comparisons; Fig. 8a). In the Y
10
11 maze, the alternation rate of nes-CrT^{-/-} mice (n = 6) was about 10% lower of that reported for nes-
12
13 CrT^{+/-} animals (n = 6; t-test, p < 0.05; Fig. 8b). We also investigated whether selective CrT
14
15 deficiency could affect hippocampal neurogenesis. Stereological analysis revealed that the number
16
17 of Ki67-positive cell was significantly lower in the DG of nes-CrT^{-/-} animal at P180 compared to
18
19 age-matched controls (n = 6 for both group; t-test, p < 0.05; Fig. 8c). These results prove that the
20
21 lack of CrT protein exclusively restricted to brain cells is sufficient to recapitulate the cognitive and
22
23 cellular defects displayed by global knock-out mice.
24
25
26
27
28
29

30 Discussion

31
32 CCDS1 is known to cause brain Cr depletion and several neurological deficits, but nothing is
33
34 known about the neurobiological basis of this disease. We performed the first analysis of
35
36 morphological, cellular and behavioral impairments in a CCDS1 mouse model. The results report
37
38 the earliest cognitive phenotype observed so far in CCDS1 mice, and a novel behavioral phenotype
39
40 consisting in enhanced stereotypies. Moreover, we found that phenotypes associated with brain
41
42 aging, including a progressive learning and memory deterioration, synaptic loss, microglial cell
43
44 activation, neurogenesis impairment and lipofuscin deposition already occurs in adult animals. The
45
46 significant differences in learning and memory performance of CrT^{-/-} mice reflected changes in
47
48 cognitive abilities *per se*: indeed, the open field test revealed that mutant mice display anxiety
49
50 levels in the range of normal values, indicating that their capacity to cope with stressful conditions
51
52 of behavioral tests is not altered.
53
54
55

56 It is essential noticing that the main organ affected in human CCDS1 is the brain, with
57
58 patients showing normal cardiac function and unaltered Cr levels in the muscle (2). In contrast,
59
60

1
2
3 CrT^{-/-} mice displayed a marked reduction of Cr also in peripheral tissues. To understand whether
4
5 the cognitive phenotype observed in CrT null mice depends on brain CrT deletion or if peripheral
6
7 factors may also play a key role, we analyzed learning and memory in a mouse model in which
8
9 CrT deletion was restricted to the brain. Our results demonstrate that Cr brain-specific depletion is
10
11 sufficient to cause a cognitive impairment indistinguishable from that of mice with ubiquitous CrT
12
13 deletion.
14

18 **The role of Cr deficiency in aging process: novel mechanistic insights**

20 An important question raised by the premature aging of CrT^{-/-} mice concerns the role of Cr
21
22 deficiency in the aging process. It is worth noting that the cognitive regression of CrT^{-/-} animals
23
24 was not paralleled by either a decrease of Cr levels in the brain tissue or a rise of GAA toxicity,
25
26 suggesting that the prolonged lack of Cr energy buffer may set in motion cellular compensatory
27
28 mechanisms leading to the gradual shutdown of brain function. We detected a significant reduction
29
30 of Cr levels in P180 CrT^{-/-} mice with respect to P30 CrT null mice only at level of muscular tissue,
31
32 indicating that the compensatory upregulation of Cr biosynthesis in the muscle declines with age.
33
34 Despite the ubiquitous pattern of CrT deletion, only few CCDS1 patients displayed an alteration of
35
36 muscular Cr levels and strength (36). Our results raise the possibility that a muscular phenotype
37
38 could occur also in patients later in life.
39
40
41
42

43 We have considered the possibility that the accelerated decline in cognitive performance in
44
45 mature CrT^{-/-} animals could be related to the documented neuroprotective (e.g., (15, 36, 38)) and
46
47 anti-apoptotic effects of Cr (39). However, when we examined neuronal density in the cerebral
48
49 cortex, we did not detect any significant reduction in the number of NeuN-positive cells either in
50
51 the PFC or in the ACC. In contrast, we found a marked impairment of hippocampal neurogenesis in
52
53 the brain of mature CrT^{-/-} mice. This was assessed by observing significantly reduced numbers of
54
55 Ki67-positive proliferating cells along with DCX-positive immature neurons in the hippocampal
56
57 DG region. These results are consistent with the notion that the creation of new neurons is an
58
59
60

1
2 energetically expensive process (40) and that the hippocampus is particularly vulnerable to
3 metabolic alterations (41). Since adult hippocampal neurogenesis plays a vital role in maintaining
4 normal cognitive processing (41, 42), an impairment of this process could conceivably compromise
5 hippocampal function and represent a key substrate of the cognitive defects seen in CrT^{-y} mice.
6
7 Accordingly, most studies indicate a correlation between a compromised neurogenic niche and
8 impaired performance in hippocampus-dependent cognitive tasks in aged mice (31).
9
10
11
12
13
14
15

16 In addition, we observed that long-term Cr deficiency induce a more subtle and specific
17 reorganization of neuronal circuits consisting in significantly lower expression of the vesicular
18 GABA transporter. This alteration, which has been detected in two brain regions fundamentally
19 involved in the processing of learning and memory tasks such as the PFC and the ACC, could be
20 mirrored by a significant dysfunction of synaptic activity leading to increased cognitive frailty. It
21 has been reported, indeed, that alterations in inhibitory interneurons contribute to cognitive deficits
22 associated with aging and neurological diseases (43, 44).
23
24
25
26
27
28
29
30
31

32 One of the principal findings of this work is the demonstration that neuroinflammation plays
33 a critical role in the progression of CrT disorder. It is apparent that Cr deficiency causes an aberrant
34 activation of microglial cells in the brain of mature CrT^{-y} animals and activated microglia may
35 release a number of cytokines and chemokines, which in turn activate many proinflammatory signal
36 transduction pathways. It is known that co-activation of proinflammatory and cytotoxic products
37 during neuroinflammation process are detrimental to neurons and may alter synaptic proteins (45).
38 Several studies, indeed, showed a significant downregulation of protein and mRNA levels of
39 synaptic markers in animal models of neuroinflammation such as a non-infectious rat model of
40 HIV-1 and rats treated with a high dose of lipopolysaccharide (46, 47). Recent evidence
41 demonstrates that neuroinflammation also negatively affects hippocampal neurogenesis (48, 49).
42
43 We could hypothesize that activated microglia-neuron crosstalk have detrimental effects on
44 hippocampal neurogenesis and brain synaptic connectivity in CrT^{-y} animals. Thus, the
45
46
47
48
49
50
51
52
53
54
55
56
57
58
59
60

1
2
3 dysregulation of microglial behavior appears to be a critical component of the negative progression
4
5 of CrT deficiency pathology.
6

7 A possible trigger of neuroinflammation is the increased concentration of damaged
8
9 macromolecules and protein aggregates as a result of an increase in oxidative stress as well as of
10
11 mitochondrial dysfunction leading to excessive generation of reactive oxygen species (ROS) and
12
13 oxidative damage to lipids, proteins and DNA. The Cr/PCr system is strongly implicated in cellular
14
15 bioenergetic function and several studies have revealed a correlation between Cr levels and
16
17 intracellular ROS inasmuch Cr exhibits antioxidant activity through either direct interaction with
18
19 oxidant species or metabolic action conferring antioxidant protection (16, 17). Accordingly, we
20
21 found an enhanced accumulation of lipofuscin in the brain of CrT^{-/-} mice that could be the result of
22
23 increased oxidative damage (50). The presence of lipofuscin can also influence important cellular
24
25 processes, such as autophagy, by inhibiting the fusion between autophagosomes and lysosomes,
26
27 thus further exacerbating the accumulation of degradation products and cognitive impairment (51).
28
29
30

31
32 Since our morphological analysis of mutant brain was all performed in adult animals, future
33
34 studies will need to check the developmental profile of markers modifications to better dissect
35
36 cellular defects underlying the onset and progression of the pathological behavioral phenotype in
37
38 CrT null mice.
39
40
41
42

43 **Impact on CCDS1 patients**

44
45 Present results have demonstrated that CrT null mice undergo to an early onset of brain aging. One
46
47 fundamental conclusion emerging from this work is that CCDS1 is a metabolic disorder associated
48
49 with early brain aging and that age should be a key factor to deal with in the clinical evaluation of
50
51 patients. It has been previously reported that patient intellectual disability becomes more
52
53 pronounced with age (6), but longitudinal studies in patients are totally lacking and little is known
54
55 about the progression of the disease.
56
57
58
59
60

1
2
3 In addition, our CrT mouse model allowed us to discover alterations of cellular and
4
5 molecular mechanisms that play a pivotal role in the generation of the CCDS1 neurological
6
7 phenotype. Mutant mice displayed alteration of GABAergic system, reduction of hippocampal
8
9 neurogenesis, marked activation of microglia, and altered oxidative metabolism, leading to a
10
11 general cognitive deterioration progressively worsening with age. This knowledge opens the
12
13 important possibility to design targeted-drug intervention protocols aimed at overcoming brain
14
15 alterations. If we could rescue brain alterations underlying CCDS1, indeed, both clinical and
16
17 behavioral amelioration should be achieved. The use of non-invasive methods for behavioral
18
19 assessment suitable for longitudinal analysis and the morphological characterization of brain
20
21 alterations in CrT^{-/y} mice set a firm background for translational studies using this model, providing
22
23 normative data and protocols necessary to validate potential treatment strategies prior to launching
24
25 costly clinical trials. Finally, our data also suggest that CrT^{-/y} animals may serve as a useful model
26
27 for exploring the mechanisms of age-related damage in the brain. A large number of
28
29 neurodevelopmental and neurological disorders, including Down syndrome, Batten disease,
30
31 progranulin deficiency, brain iron dysregulation, have been associated with early brain aging (52–
32
33 55). Thus, a better understanding of factors that accelerate age-related deterioration of cognitive
34
35 performance is critical both for improving the likelihood for successful aging and for revealing
36
37 pathological changes of translational value.
38
39
40
41
42
43

44 **Material and methods**

47 **Animals**

49 As CrT deficiency is an X-linked pathology, male mice were selected for this study. CrT^{-/y} and
50
51 CrT^{+/y} mice on a C57BL/6 J background were generated as described previously (11). Animals
52
53 were maintained at 22°C under a 12-h light–dark cycle (average illumination levels of 1.2 cd/m²).
54
55 Food (4RF25 GLP Certificate, Mucedola) and water were available *ad libitum*. To target CrT
56
57 deletion to neuronal and glial cells of the central nervous system we used a mouse (35) expressing
58
59
60

1
2
3 Cre recombinase under the Nestin promoter (Nestin:Cre). CrT^{+/fl} females were crossed with
4
5 Nestin:Cre male mice to generate a mouse line carrying the floxed CrT and Nestin:Cre alleles. Mice
6
7 with three genotypes were used as experimental animals: mice carrying the brain specific deletion
8
9 of CrT (Nestin:Cre-CrT^{-y}, nes-CrT^{-y}), mice expressing the floxed allele but not Cre-recombinase
10
11 (CrT^{fl/y}), and mice expressing Cre-recombinase but not carrying the floxed allele (Nestin:Cre-
12
13 CrT^{+y}, nes-CrT^{+y}). These genotypes were obtained in the same litters. Since CrT^{fl/y} mice did not
14
15 display any difference in Cr levels with respect to nes-CrT^{+y} animals, we performed behavioral and
16
17 anatomical investigation only in the other two experimental groups. All experiments were carried
18
19 out in accordance with the European Communities Council Directive of 24 November 1986
20
21 (86/609/EEC) and were approved by the Italian Ministry of Health (authorization number
22
23 259/2016-PR).

24 25 26 27 28 **Detection of *Slc6a8* mutation by PCR**

29
30 Genomic DNA was isolated from mouse tail using a kit, and the protocol suggested by the
31
32 manufacturer (DNeasy Blood & Tissue Kit, Qiagen, USA). DNA was amplified for CrT mutant and
33
34 wild-type (WT) allele using a standard PCR protocol with the following primers:

35
36 F:AGGTTTCCTCAGGTTATAGAGA; R:CCCTAGGTGTATCTAACATCT; R1:

37
38 TCGTGGTATCGTTATGCGCC. Primers for Cre recombinase expression were: F:

39
40 AACGCACTGATTTCGACC; R: CAACACCATTTTTCTGACCC. For PCR amplification we

41
42 used 300 ng of DNA in a 25 µL reaction volume containing 0.2 mM of each dNTP, 2 µM of F
43
44 primer, 1 µM of R, 1 µM of R1 primer and 0.5 U/µL Red Taq DNA polymerase (Sigma-Aldrich,
45
46 Italy). The PCR conditions were as follows: 94°C for 4 min followed by 37 cycles at 94°C for 30 s,
47
48 58°C for 30 s, 72°C for 40 s and a final extension at 72°C for 7 min. Amplicons were separated
49
50 using 2% agarose gel and visualized under UV light after staining with Green Gel Plus (Fisher
51
52 Molecular Biology, Rome, Italy). Amplicon sizes were: WT allele = 462 bp; mutant allele = 371
53
54 bp; Cre allele = 310 bp.
55
56
57
58
59
60

Behavioral testing

The testing order for behavioral assessment performed in the same animals consisted of: open field (1 day duration), object recognition test (ORT) at 1h (1 day), ORT at 24h (3 days), Y maze (1 day), Morris water maze (MWM) with hidden platform (7 days), rotarod (1 day), three chamber social test (1 day) and self-grooming (1 day). The mice were tested on one task at a time with the next behavioral test starting at least 1 days after the completion of the previous one. While open field, ORT, Y maze, rotarod and self-grooming were longitudinally administered to the same animals, MWM was performed in separate groups of animals at the different ages tested. Y maze has been also used to test cognitive functions in juvenile animals (P28). Social behavior has been tested only in 6-month-old animals. In order to reduce the circadian effects, behavioral tests were performed during the same time interval each day (14:00–18:00h; light phase). All behavioral tests were conducted in blind with respect to the genotype of animals. Animals not performing the task required were excluded from the analysis. Mice were weighed at the end of experiments.

Open field and object recognition test (ORT)

The apparatus consisted of a square arena ($60 \times 60 \times 30$ cm) constructed in poly(vinyl chloride) with black walls and a white floor. The mice received one session of 10-min duration in the empty arena to habituate them to the apparatus and test room. Animal position was continuously recorded by a video tracking system (Noldus Ethovision XT). In the recording software an area corresponding to the center of the arena (a central square 30×30 cm), and a peripheral region (corresponding to the remaining portion of the arena) were defined. The total movement of the animal and the time spent in the center or in the periphery area were automatically computed. Mouse activity during this habituation session was analyzed for evaluating the behavior in the open field arena. The ORT consisted of two phases: sample and testing phase. During the sample phase, two identical objects were placed in diagonally opposite corners of the arena, approximately 6 cm

1
2
3 from the walls, and mice were allowed 10 min to explore the objects, then they were returned to
4 their cage. The objects to be discriminated were made of plastic, metal, or glass material and were
5 too heavy to be displaced by the mice. The testing phase was performed either 1h or 24h after the
6 sample phase. One of the two familiar objects was replaced with a new one, while the other object
7 was replaced by an identical copy. The objects were placed in the same locations as the previous
8 ones. The mice were allowed to explore objects for 5 min. To avoid possible preferences for one of
9 two objects, the choice of the new and old object and the position of the new one were randomized
10 among animals. The amount of time spent exploring each object (nose sniffing and head orientation
11 within <1.0 cm) was recorded and evaluated by the experimenter blind to the mouse genotype.

12
13
14
15
16
17
18
19
20
21
22
23
24
25
26
27
28
29
30
31
32
33
34
35
36
37
38
39
40
41
42
43
44
45
46
47
48
49
50
51
52
53
54
55
56
57
58
59
60
Arena and objects were cleaned with 10% ethanol between trials to stop the build-up of olfactory
cues. Mice exploring the two objects for less than 10 s during the sample phase were excluded from
testing. A discrimination index was computed as $DI = (T_{\text{new}} - T_{\text{old}})/(T_{\text{new}} + T_{\text{old}})$, where T_{new} is
the time spent exploring the new object, and T_{old} is the time spent exploring the old one (11).

Y maze spontaneous alternation

We used a Y-shaped maze with three symmetrical grey solid plastic arms at a 120-degree angle (26
cm length, 10 cm width, and 15 cm height). Mice were placed in the center of the maze and allowed
to freely explore the maze for 8 minutes. The apparatus was cleaned with 10% ethanol between
trials to avoid the build-up of odor traces. All sessions were video-recorded (Noldus Ethovision XT)
for offline blind analysis. The arm entry was defined as all four limbs within the arm. A triad was
defined as a set of three arm entries, when each entry was to a different arm of the maze. The
number of arm entries and the number of triads were recorded in order to calculate the alternation
percentage (generated by dividing the number of triads by the number of possible alternations and
then multiplying by 100; (11).

Morris water maze

1
2
3 Mice were trained for four trials per day and for a total of 7 days (11) in a circular water tank, made
4
5 from grey polypropylene (diameter, 120 cm; height, 40 cm), filled to a depth of 25 cm with water
6
7 (23°C) rendered opaque by the addition of a non-toxic white paint. Four positions around the edge
8
9 of the tank were arbitrarily designated North (N), South (S), East (E), and West (W), which
10
11 provided four alternative start positions and also defined the division of the tank into four
12
13 quadrants, i.e., NE, SE, SW, and NW. A square clear Perspex escape platform (11 × 11 cm) was
14
15 submerged 0.5 cm below the water surface and placed at the midpoint of one of the four quadrants.
16
17 The hidden platform remained in the same quadrant during training, while the start positions (N, S,
18
19 E, or W) were randomized across trials. The pool was situated in a room containing extra-maze
20
21 cues that provide specific visual reference points for locating the submerged platform. Mice were
22
23 allowed up to 60 s to locate the escape platform, and their swimming paths were automatically
24
25 recorded by the Noldus Ethovision system. If the mouse failed to reach the platform within 60 s, the
26
27 trial was terminated, and the mouse was guided onto the platform for 15 s. On the last trial of the
28
29 last training day, mice received a probe trial, during which the escape platform was removed from
30
31 the tank and the swimming paths were recorded over 60 s while mice searched for the missing
32
33 platform. The swimming paths were recorded and analyzed with the Noldus Ethovision system.
34
35
36
37
38
39
40

41 **Rotarod**

42
43 Motor coordination and abilities were assessed using the rotarod test as described in (56). Animals
44
45 were placed on a drum with increasing rotation speed from 4 to 40 rpm. The time spent on the drum
46
47 was recorded by an automated unit, which stops as the mouse fall. Motor abilities were assessed by
48
49 conducting the test for four consecutive times with an interval of 5 min in the same day.
50
51
52
53

54 **Three-chamber social test**

55
56 The three-chamber paradigm test has been successfully employed to study sociability and
57
58 preference for social novelty in several mutant mouse lines. "Sociability" is defined as propensity to
59
60

1
2
3 spend time with a conspecific, as compared to time spent alone in an identical but empty chamber;
4
5 "preference for social novelty" is defined as propensity to spend time with a new mouse rather than
6
7 with a familiar mouse (57). We adapted the protocol reported in (58). The apparatus consisted in a
8
9 rectangular, three-chamber box made from clear Plexiglas (72 cm wide × 50 cm length × 33 high).
10
11 Each chamber is 24 x 50 cm and the dividing walls are made from clear Plexiglas, with an open
12
13 middle section, which allows free access to each chamber. Two identical, wire cup-like containers
14
15 with removable lids were placed inside the apparatus, one in each side chamber. Each container was
16
17 made of metal wires allowing for air exchange between the interior and exterior of the cup but small
18
19 enough to prevent direct physical interactions between the inside animal and the subject mouse.
20
21 Two classes of mouse were used in this experiment, one acting as a control, naïve animal, while the
22
23 other is the test subject. The control mouse was a mouse of the same background, age, gender and
24
25 weight, without any prior contact with the subject mouse. Two control mice were required per
26
27 experiment, one used for session I (Stranger 1) and another for session II (Stranger 2). The same
28
29 control mice were used between trials. Control mice were gradually habituated to wire-cup housing
30
31 in the three-chamber box for 4 days (30 min per day) before the starting of test session. After 10
32
33 min of habituation in the arena with empty wire cups of the subject mouse, we placed Stranger 1
34
35 inside one of the wire cups. The subject mice were allowed to explore each of the three chambers
36
37 for 10 min (session I). Animal position was continuously recorded by a video tracking system
38
39 (Noldus Ethovision XT). The amount of time spent exploring each wire cup was recorded and
40
41 evaluated by the experimenter blind to the mouse genotype. A discrimination index was computed
42
43 as $DI = (T_{soc} - T_{obj}) / (T_{soc} + T_{obj})$, where T_{soc} is the time spent exploring the cup housing the
44
45 Stranger 1, and T_{obj} is the time spent exploring the other cup. In session II we placed Stranger 2
46
47 inside the wire cup in the opposite side chamber. Duration of session II was 10 min and we
48
49 calculated the same DI described above, differentiating the exploration time of the subject mouse
50
51 between Stranger 1 and Stranger 2. The placement of Stranger 1 and Stranger 2 in the left or right
52
53
54
55
56
57
58
59
60

1
2
3 side of the box was randomized between trials. Arena and wire cups were cleaned with 10% ethanol
4
5 between trials to prevent olfactory cue bias.
6
7
8

9 10 **Self-grooming**

11 Mice were scored for spontaneous grooming behaviors as described earlier (59). Each mouse was
12 placed individually into a clean, empty, standard mouse cage (27 length × 20 cm wide × 15 cm
13 high) without bedding. Animal behaviors were videotaped for 20 min. After a 10-min habituation
14 period in the test cage, each mouse was scored with a stopwatch for 10 min for cumulative time
15 spent grooming all body regions.
16
17
18
19
20
21
22
23

24 **Biochemical analysis**

25 For Cr and GAA assay, mouse tissues, immediately frozen on dry ice and stored at -80°C until the
26 analysis, were homogenized in 0.7 ml PBS buffer (Sigma-Aldrich, Italy) at 4°C using a ultrasonic
27 disruptor (Microson Heat System, NY, USA) for brain or a glass manual homogenizer (VWR, Italy)
28 for kidney, heart and muscle. After centrifugation (600 × g for 10 min at 4°C) an aliquot of the
29 homogenate (50 µl) was assayed for protein content and the supernatant used for Cr assay as
30 previously described (60). Briefly, 50 µl of saturated sodium hydrogen carbonate and 50 µl of a
31 mixture containing 2- phenylbutyric acid (I.S.) in toluene (6.09 mmol/l; Sigma-Aldrich, Italy) were
32 added to 200 µl of homogenate or to 100 µl of serum and urine, respectively. After adding 1 ml of
33 toluene and 50 µl of hexafluoro-2,4-pentanedione (Sigma-Aldrich, Italy) to form bis-
34 trifluoromethyl- pyrimidine derivatives, the mixture was stirred overnight at 80°C. The organic
35 layer was centrifuged, dried under nitrogen and 2 µl of the residue derivatized at room temperature
36 with 100 µl of BSTFA+TMCS (Sigma-Aldrich, Italy) injected into the Gas Chromatography/Mass
37 Spectrometry (GC/MS) instrument. GC analyses were performed using an Agilent 6890N GC
38 equipped with an HP5MS capillary column (0.25 mm × 30 m, film thickness 0.25 µm) and an
39 Agilent mass spectrometer 5973N (Agilent Technologies, Italy). The mass spectrometer was set in
40
41
42
43
44
45
46
47
48
49
50
51
52
53
54
55
56
57
58
59
60

1
2
3 EI- single ion monitoring mode (SIM). The ions with m/z of 192 for I.S., 258 for Cr and 225 for
4
5 guanidinoacetic acid (GAA) were used for calculation of the metabolites, using standard curves
6
7 ranging 5–90 $\mu\text{mol/L}$ and 0.30–6 $\mu\text{mol/L}$ for Cr and GAA, respectively. Data were processed by
8
9 the G1701DA MSD ChemStation software. All the aqueous solutions were prepared using ultrapure
10
11 water produced by a Millipore system.
12
13

14 15 16 **Immunohistochemistry**

17
18 Animals were perfused transcardially with 4% paraformaldehyde in phosphate buffer. Brains were
19
20 post-fixed and impregnated with 30% sucrose in phosphate buffered saline (PBS). Coronal brain
21
22 sections (40 μm) were cut on a freezing microtome and collected in PBS before being processed for
23
24 immunohistochemistry. After a blocking step, free-floating slices were incubated O/N at 4°C in a
25
26 solution of primary antibody (NeuN, Millipore, 1:500; Ki67, Abcam, 1:400; DCX, Abcam, 1:200;
27
28 vGlut1, Synaptic System, 1:500; vGAT, Synaptic System, 1:1,000; Iba-1, Wako, 1:400) and
29
30 antigen-antibody interaction was revealed with suitable Alexa Fluor-conjugated secondary
31
32 antibodies (1:400, Invitrogen). Immunostaining for Ki67 involved an additional treatment with
33
34 sodium citrate for antigen retrieval. Sections were then counterstained with Hoechst dye (1: 500,
35
36 Sigma), mounted on microscope slides and coverslipped using Vectashield mounting medium for
37
38 fluorescence (Vector Laboratories Inc.).
39
40
41
42
43
44

45 **Image analysis**

46
47 *NeuN and Iba1*- To quantify the density of neuronal and microglial cells in the cerebral cortex we
48
49 used the StereoInvestigator software (MicroBrightField) equipped with motorized X–Y sensitive
50
51 stage and video camera connected to a computerized image analysis system. NeuN-positive cells
52
53 were counted using 20x magnification and sampling boxes (250 x 250 x 40 μm) located in both
54
55 superficial and deep layers of PFC and ACC cortex. Iba1-positive cells were counted using 40x
56
57 magnification and sampling boxes (250 x 250 x 40 μm) located in both superficial and deep layers
58
59
60

1
2
3 of PFC cortex. Cell density was calculated by averaging values obtained from at least 6-8 counting
4
5 boxes per animal. *Ki67 and DCX*- Examination of Ki67 and DCX-positively labelled cells was
6
7 confined to the hippocampal dentate gyrus (DG), specifically to the granule cell layer (GCL) and
8
9 the subgranular zone of the hippocampus defined as a two-cell body-wide zone along the border
10
11 between the GCL and hilus. Quantification of Ki67 or DCX-immunoreactive cells was conducted
12
13 from 1-in-6 series of immunolabelled sections using 20x magnification and spanning the
14
15 rostrocaudal extent of DG. All immunostained sections were analysed using the StereoInvestigator
16
17 software. The reference volume was determined as the sum of the traced areas multiplied by the
18
19 distance between the sampled sections. Densities of immunopositive cells were then calculated by
20
21 dividing the number of positive cells by the reference volume. Numbers of positively labelled
22
23 neurons were normalized as density per unit of volume (mm^3). *vGlut1 and vGAT*- To quantify the
24
25 density of vGlut1- and vGAT-positive puncta, the parameters of acquisition (laser intensity, gain,
26
27 offset) were optimized at the beginning of the acquisition and then held constant throughout image
28
29 acquisition. All sections were acquired in random order in a single session to minimize fluctuation
30
31 in laser output and degradation of fluorescence. We imaged superficial and deep layers of PFC and
32
33 ACC on a Zeiss laser-scanning Apotome microscope using a 63x oil immersion objective. For each
34
35 section, we imaged serial optical sections at 0.33 μm intervals for a total of at least 15 optical
36
37 sections (5 μm). From each animal we imaged 6 sections (3 in superficial layers and 3 in deep
38
39 layers). Maximum intensity projections (MIPs) were generated from the group of 5 consecutive
40
41 sections yielding the higher mean pixel intensity. These MIPs were imported in ImageJ and
42
43 quantified using Puncta analyzer plugin (61). The number of positive puncta was measured within
44
45 the entire acquired area.
46
47
48
49
50

51 52 53 54 **Determination of lipofuscin accumulation by autofluorescence**

55
56 Coronal brain sections were mounted on microscope slides and coverslipped using Vectashield
57
58 mounting medium for fluorescence (Vector Laboratories Inc.). We imaged hippocampal DG on a
59
60

1
2
3 Zeiss laser-scanning Apotome microscope using a 40x oil immersion objective. The parameters of
4 acquisition were optimized at the beginning of the experiment and then held constant. Lipofuscin
5 level was measured as the presence of autofluorescence at 550 nm in the region of interest. For each
6
7 section, we imaged serial optical sections at 0.5 μm intervals for a total of at least 80 optical
8
9 sections (40 μm). From each animal we imaged 3-4 sections. MIPs were generated from the group
10
11 of 5 consecutive sections yielding the higher mean pixel intensity. These MIPs were imported in
12
13 ImageJ and quantified using Threshold plugin. The area of positive puncta and mean pixel intensity
14
15 were measured within the entire acquired area.
16
17
18
19
20

21 **Statistical analysis**

22
23 All statistical analyses were performed using SigmaStat Software. Differences between two groups
24 were assessed with a two-tailed t test. The significance of factorial effects and differences among
25
26 more than two groups were evaluated with ANOVA/RM ANOVA followed by Holm-Sidak test.
27
28 Rank transformation was exploited for data not normally distributed. The level of significance was
29
30 $p < 0.05$.
31
32
33
34
35
36

37 **Acknowledgements:** We thank Francesca Biondi for animal care and Cristina Pitzalis for test
38
39 representative illustrations.
40
41
42

43
44 **Conflict of Interest Statement:** The authors declare no conflict of interest.
45
46
47

48 **References**

- 49
50
51 1. Wallimann, T., Tokarska-Schlattner, M. and Schlattner, U. (2011) The creatine kinase system
52
53 and pleiotropic effects of creatine. *Amino Acids*, **40**, 1271–1296.
54
55
56
57
58
59
60

- 1
2
3 2. Joncquel-Chevalier Curt, M., Voicu, P.-M., Fontaine, M., Dessein, A.-F., Porchet, N., Mention-
4 Mulliez, K., Dobbelaere, D., Soto-Ares, G., Cheillan, D. and Vamecq, J. (2015) Creatine
5 biosynthesis and transport in health and disease. *Biochimie*, **119**, 146–165.
6
7
8
9
- 10 3. Item, C. B., Stöckler-Ipsiroglu, S., Stromberger, C., Mühl, A., Alessandri, M. G., Bianchi, M. C.,
11 Tosetti, M., Fornai, F. and Cioni, G. (2001) Arginine:glycine amidinotransferase deficiency:
12 the third inborn error of creatine metabolism in humans. *Am. J. Hum. Genet.*, **69**, 1127–1133.
13
14
15
16
17
- 18 4. Stöckler, S., Holzbach, U., Hanefeld, F., Marquardt, I., Helms, G., Requart, M., Hänicke, W. and
19 Frahm, J. (1994) Creatine deficiency in the brain: a new, treatable inborn error of metabolism.
20 *Pediatr. Res.*, **36**, 409–413.
21
22
23
24
- 25 5. Salomons, G. S., van Dooren, S. J., Verhoeven, N. M., Cecil, K. M., Ball, W. S., Degrauw, T. J.
26 and Jakobs, C. (2001) X-linked creatine-transporter gene (SLC6A8) defect: a new creatine-
27 deficiency syndrome. *Am. J. Hum. Genet.*, **68**, 1497–1500.
28
29
30
31
32
- 33 6. van de Kamp, J. M., Mancini, G. M. and Salomons, G. S. (2014) X-linked creatine transporter
34 deficiency: clinical aspects and pathophysiology. *J. Inherit. Metab. Dis.*, **37**, 715–733.
35
36
37
38
- 39 7. Mak, C. S. W., Waldvogel, H. J., Dodd, J. R., Gilbert, R. T., Lowe, M. T. J., Birch, N. P., Faull,
40 R. L. M. and Christie, D. L. (2009) Immunohistochemical localisation of the creatine
41 transporter in the rat brain. *Neuroscience*, **163**, 571–585.
42
43
44
45
- 46 8. Braissant, O., Henry, H., Béard, E. and Uldry, J. (2011) Creatine deficiency syndromes and the
47 importance of creatine synthesis in the brain. *Amino Acids*, **40**, 1315–1324.
48
49
50
51
- 52 9. Torremans, A., Marescau, B., Possemiers, I., Van Dam, D., D’Hooge, R., Isbrandt, D. and De
53 Deyn, P. P. (2005) Biochemical and behavioural phenotyping of a mouse model for GAMT
54 deficiency. *J. Neurol. Sci.*, **231**, 49–55.
55
56
57
58
59
60

- 1
2
3 10. Skelton, M. R., Schaefer, T. L., Graham, D. L., Degrauw, T. J., Clark, J. F., Williams, M. T. and
4
5 Vorhees, C.V. (2011) Creatine transporter (CrT; Slc6a8) knockout mice as a model of human
6
7 CrT deficiency. *PLoS One*, **6**, e16187.
8
9
10
11 11. Baroncelli, L., Alessandri, M. G., Tola, J., Putignano, E., Migliore, M., Amendola, E., Gross,
12
13 C., Leuzzi, V., Cioni, G. and Pizzorusso, T. (2014) A novel mouse model of creatine
14
15 transporter deficiency. *F1000Res.*, **3**, 228.
16
17
18 12. Choe, C. U., Nabuurs, C., Stockebrand, M. C., Neu, A., Nunes, P., Morellini, F., Sauter, K.,
19
20 Schillemeit, S., Hermans-Borgmeyer, I., Marescau, B., *et al.* (2013) L-arginine:glycine
21
22 amidinotransferase deficiency protects from metabolic syndrome. *Hum. Mol. Genet.*, **22**, 110–
23
24 123.
25
26
27
28 13. Nabuurs, C. I., Choe, C. U., Veltien, A., Kan, H. E., van Loon, L. J. C., Rodenburg, R. J. T.,
29
30 Matschke, J., Wieringa, B., Kemp, G. J., Isbrandt, D., *et al.* (2013) Disturbed energy
31
32 metabolism and muscular dystrophy caused by pure creatine deficiency are reversible by
33
34 creatine intake. *J. Physiol.*, **591**, 571–592.
35
36
37
38 14. Alcaide, P., Merinero, B., Ruiz-Sala, P., Richard, E., Navarrete, R., Arias, A., Ribes, A., Artuch,
39
40 R., Campistol, J., Ugarte, M., *et al.* (2011) Defining the pathogenicity of creatine deficiency
41
42 syndrome. *Hum. Mutat.*, **32**, 282–291.
43
44
45
46 15. Bender, A., Beckers, J., Schneider, I., Hölter, S. M., Haack, T., Ruthsatz, T., Vogt-Weisenhorn,
47
48 D. M., Becker, L., Genius, J., Rujescu, D., *et al.* (2008) Creatine improves health and survival
49
50 of mice. *Neurobiol. Aging*, **29**, 1404–1411.
51
52
53
54 16. Lawler, J. M., Barnes, W. S., Wu, G., Song, W. and Demaree, S. (2002) Direct antioxidant
55
56 properties of creatine. *Biochem. Biophys. Res. Commun.*, **290**, 47–52.
57
58
59
60

- 1
2
3 17. Sestili, P., Martinelli, C., Colombo, E., Barbieri, E., Potenza, L., Sartini, S. and Fimognari, C.
4
5 (2011) Creatine as an antioxidant. *Amino Acids*, **40**, 1385–1396.
6
7
8 18. McMorris, T., Mielcarz, G., Harris, R. C., Swain, J. P. and Howard, A. (2007) Creatine
9
10 supplementation and cognitive performance in elderly individuals. *Neuropsychol. Dev. Cogn.*
11
12 *B Aging Neuropsychol. Cogn.*, **14**, 517–528.
13
14
15 19. van de Kamp, J. M., Betsalel, O. T., Mercimek-Mahmutoglu, S., Abulhoul, L., Grünewald, S.,
16
17 Anselm, I., Azzouz, H., Bratkovic, D., de Brouwer, A., Hamel, B., *et al.* (2013) Phenotype and
18
19 genotype in 101 males with X-linked creatine transporter deficiency. *J. Med. Genet.*, **50**, 463–
20
21 472.
22
23
24
25 20. Laakso, M. P., Hiltunen, Y., Könönen, M., Kivipelto, M., Koivisto, A., Hallikainen, M. and
26
27 Soininen, H. (2003) Decreased brain creatine levels in elderly apolipoprotein E epsilon 4
28
29 carriers. *J. Neural Transm.*, **110**, 267–275.
30
31
32
33 21. Smith, R. N., Agharkar, A. S. and Gonzales, E. B. (2014) A review of creatine supplementation
34
35 in age-related diseases: more than a supplement for athletes. *F1000Res.*, **3**, 222.
36
37
38 22. Albani, S. H., McHail, D. G. and Dumas, T. C. (2014) Developmental studies of the
39
40 hippocampus and hippocampal-dependent behaviors: Insights from interdisciplinary studies
41
42 and tips for new investigators. *Neurosci. Biobehav. Rev.*, **43**, 183–190.
43
44
45
46 23. Etherton, M. R., Blaiss, C. A., Powell, C. M. and Sudhof, T. C. (2009) Mouse neurexin-1
47
48 deletion causes correlated electrophysiological and behavioral changes consistent with
49
50 cognitive impairments. *Proceedings of the National Academy of Sciences*, **106**, 17998–18003.
51
52
53
54 24. Rothwell, P. E., Fuccillo, M. V., Maxeiner, S., Hayton, S. J., Gokce, O., Lim, B. K., Fowler, S.
55
56 C., Malenka, R. C. and Südhof, T. C. (2014) Autism-associated neuroligin-3 mutations
57
58 commonly impair striatal circuits to boost repetitive behaviors. *Cell*, **158**, 198–212.
59
60

- 1
2
3 25. Fuccillo, M. V. (2016) Striatal Circuits as a Common Node for Autism Pathophysiology. *Front.*
4
5 *Neurosci.*, **10**, 27.
6
7
8 26. Bano, D., Agostini, M., Melino, G. and Nicotera, P. (2011) Ageing, neuronal connectivity and
9
10 brain disorders: an unsolved ripple effect. *Mol. Neurobiol.*, **43**, 124–130.
11
12
13 27. Leuzzi, V., Mastrangelo, M., Battini, R. and Cioni, G. (2013) Inborn errors of creatine
14
15 metabolism and epilepsy. *Epilepsia*, **54**, 217–227.
16
17
18 28. von Bernhardt, R., Eugenín-von Bernhardt, L. and Eugenín, J. (2015) Microglial cell
19
20 dysregulation in brain aging and neurodegeneration. *Front. Aging Neurosci.*, **7**, 124.
21
22
23 29. Matt, S. M. and Johnson, R. W. (2016) Neuro-immune dysfunction during brain aging: new
24
25 insights in microglial cell regulation. *Curr. Opin. Pharmacol.*, **26**, 96–101.
26
27
28 30. Hefendehl, J. K., Neher, J. J., Sühs, R. B., Kohsaka, S., Skodras, A. and Jucker, M. (2014)
29
30 Homeostatic and injury-induced microglia behavior in the aging brain. *Aging Cell*, **13**, 60–69.
31
32
33 31. Lee, S. W., Clemenson, G. D. and Gage, F. H. (2012) New neurons in an aged brain. *Behav.*
34
35 *Brain Res.*, **227**, 497–507.
36
37
38 32. Dunlop, R. A., Brunk, U. T. and Rodgers, K. J. (2009) Oxidized proteins: mechanisms of
39
40 removal and consequences of accumulation. *IUBMB Life*, **61**, 522–527.
41
42
43 33. Terman, A. and Brunk, U. T. (2006) Oxidative stress, accumulation of biological ‘garbage’, and
44
45 aging. *Antioxid. Redox Signal.*, **8**, 197–204.
46
47
48 34. Assunção, M., Santos-Marques, M. J., Carvalho, F., Lukoyanov, N. V. and Andrade, J. P.
49
50 (2011) Chronic green tea consumption prevents age-related changes in rat hippocampal
51
52 formation. *Neurobiol. Aging*, **32**, 707–717.
53
54
55
56
57
58
59
60

- 1
2
3 35. Tronche, F., Kellendonk, C., Kretz, O., Gass, P., Anlag, K., Orban, P.C., Bock, R., Klein, R.,
4
5 Schütz, G. (1999) Disruption of the glucocorticoid receptor gene in the nervous system results
6
7 in reduced anxiety. *Nat. genet.*, **23**, 99-103.
8
9
10 36. Puusepp, H., Kall, K., Salomons, G.S., Talvik, I., Männamaa, M., Rein, R., Jakobs, C., Öunap,
11
12 K. (2010) The screening of SLC6A8 deficiency among Estonian families with X-linked mental
13
14 retardation. *J Inherit Metab Dis*, **33**, S5-11.
15
16
17 37. Matthews, R. T., Ferrante, R. J., Klivenyi, P., Yang, L., Klein, A. M., Mueller, G., Kaddurah-
18
19 Daouk, R. and Beal, M. F. (1999) Creatine and cyclocreatine attenuate MPTP neurotoxicity.
20
21 *Exp. Neurol.*, **157**, 142–149.
22
23
24 38. Sullivan, P. G., Geiger, J. D., Mattson, M. P. and Scheff, S. W. (2000) Dietary supplement
25
26 creatine protects against traumatic brain injury. *Ann. Neurol.*, **48**, 723–729.
27
28
29 39. O’Gorman, E., Beutner, G., Dolder, M., Koretsky, A. P., Brdiczka, D. and Wallimann, T.
30
31 (1997) The role of creatine kinase in inhibition of mitochondrial permeability transition. *FEBS*
32
33 *Lett.*, **414**, 253–257.
34
35
36
37 40. Kempermann, G. (2015) Activity Dependency and Aging in the Regulation of Adult
38
39 Neurogenesis. *Cold Spring Harb. Perspect. Biol.*, **7**.
40
41
42 41. Bartsch, T. and Wulff, P. (2015) The hippocampus in aging and disease: From plasticity to
43
44 vulnerability. *Neuroscience*, **309**, 1–16.
45
46
47 42. Christian, K. M., Song, H. and Ming, G. L. (2014) Functions and dysfunctions of adult
48
49 hippocampal neurogenesis. *Annu. Rev. Neurosci.*, **37**, 243–262.
50
51
52
53
54
55
56
57
58
59
60

- 1
2
3 43. Bories, C., Husson, Z., Guitton, M. J. and De Koninck, Y. (2013) Differential balance of
4
5 prefrontal synaptic activity in successful versus unsuccessful cognitive aging. *J. Neurosci.*, **33**,
6
7 1344–1356.
8
9
- 10 44. McQuail, J. A., Frazier, C. J. and Bizon, J. L. (2015) Molecular aspects of age-related cognitive
11
12 decline: the role of GABA signaling. *Trends Mol. Med.*, **21**, 450–460.
13
14
- 15 45. Rao, J. S., Matthew, K., Hyung-Wook, K., Rapoport, S. I. and Reese, E. A. (2012)
16
17 Neuroinflammation and Synaptic Loss. *Neurochem. Res.*, **37**, 903–910.
18
19
- 20 46. Rao, J. S., Kim, H. W., Kellom, M., Greenstein, D., Chen, M., Kraft, A. D., Harry, G. J.,
21
22 Rapoport, S. I. and Basselin, M. (2011) Increased neuroinflammatory and arachidonic acid
23
24 cascade markers, and reduced synaptic proteins, in brain of HIV-1 transgenic rats. *J.*
25
26 *Neuroinflammation*, **8**, 101.
27
28
- 29 47. Kellom, M., Basselin, M., Keleshian, V. L., Chen, M., Rapoport, S.I. and Rao, J. S. (2012)
30
31 Dose-dependent changes in neuroinflammatory and arachidonic acid cascade markers with
32
33 synaptic marker loss in rat lipopolysaccharide infusion model of neuroinflammation. *BMC*
34
35 *Neurosci.*, **13**, 50.
36
37
- 38 48. Sierra, A., Beccari, S., Diaz-Aparicio, I., Encinas, J. M., Comeau, S. and Tremblay, M. È.
39
40 (2014) Surveillance, phagocytosis, and inflammation: how never-resting microglia influence
41
42 adult hippocampal neurogenesis. *Neural Plast.*, **2014**, 610343.
43
44
- 45 49. Ryan, S. M. and Nolan, Y. M. (2016) Neuroinflammation negatively affects adult hippocampal
46
47 neurogenesis and cognition: can exercise compensate? *Neurosci. Biobehav. Rev.*, **61**, 121–131.
48
49
- 50 50. Höhn, A. and Grune, T. (2013) Lipofuscin: formation, effects and role of macroautophagy.
51
52
53
54
55
56
57
58
59
60

- 1
2
3 51. Brandenstein, L., Schweizer, M., Sedlacik, J., Fiehler, J., Storch, S. (2016) Lysosomal
4
5 dysfunction and impaired autophagy in a novel mouse model deficient for the lysosomal
6
7 membrane protein Cln7. *Hum. Mol. Genet.*, **25**, 777–791.
8
9
10 52. Kopra, O., Vesa, J., von Schantz, C., Manninen, T., Minye, H., Fabritius, A. L., Rapola, J., van
11
12 Diggelen, O. P., Saarela, J., Jalanko, A., *et al.* (2004) A mouse model for Finnish variant late
13
14 infantile neuronal ceroid lipofuscinosis, CLN5, reveals neuropathology associated with early
15
16 aging. *Hum. Mol. Genet.*, **13**, 2893–2906.
17
18
19 53. Ahmed, Z., Sheng, H., Xu, Y. F., Lin, W. L., Innes, A. E., Gass, J., Yu, X., Wuertzer, C. A.,
20
21 Hou, H., Chiba, S., *et al.* (2010) Accelerated lipofuscinosis and ubiquitination in granulin
22
23 knockout mice suggest a role for progranulin in successful aging. *Am. J. Pathol.*, **177**, 311–
24
25 324.
26
27
28
29 54. Maccarinelli, F., Pagani, A., Cozzi, A., Codazzi, F., Di Giacomo, G., Capoccia, S., Rapino, S.,
30
31 Finazzi, D., Politi, L. S., Cirulli, F., *et al.* (2015) A novel neuroferritinopathy mouse model
32
33 (FTL 498InsTC) shows progressive brain iron dysregulation, morphological signs of early
34
35 neurodegeneration and motor coordination deficits. *Neurobiol. Dis.*, **81**, 119–133.
36
37
38
39 55. Head, E., Lott, I. T., Wilcock, D. M. and Lemere, C. A. (2016) Aging in Down Syndrome and
40
41 the Development of Alzheimer’s Disease Neuropathology. *Curr. Alzheimer Res.*, **13**, 18–29.
42
43
44
45 56. Lonetti, G., Angelucci, A., Morando, L., Boggio, E. M., Giustetto, M. and Pizzorusso, T. (2010)
46
47 Early environmental enrichment moderates the behavioral and synaptic phenotype of MeCP2
48
49 null mice. *Biol. Psychiatry*, **67**, 657–665.
50
51
52
53 57. Moy, S. S., Nadler, J. J., Perez, A., Barbaro, R. P., Johns, J. M., Magnuson, T. R., Piven, J. and
54
55 Crawley, J.N. (2004) Sociability and preference for social novelty in five inbred strains: an
56
57 approach to assess autistic-like behavior in mice. *Genes Brain Behav.*, **3**, 287–302.
58
59
60

- 1
2
3 58. Kaidanovich-Beilin, O., Lipina, T., Vukobradovic, I., Roder, J. and Woodgett, J. R. (2011)
4
5 Assessment of social interaction behaviors. *J. Vis. Exp.*, 10.3791/2473.
6
7
8 59. McFarlane, H. G., Kusek, G. K., Yang, M., Phoenix, J. L., Bolivar, V. J. and Crawley, J. N.
9
10 (2008) Autism-like behavioral phenotypes in BTBR T+tf/J mice. *Genes Brain Behav.*, 7, 152–
11
12 163.
13
14
15 60. Alessandri, M. G., Celati, L., Battini, R., Casarano, M. and Cioni, G. (2005) Gas
16
17 chromatography/mass spectrometry assay for arginine: glycine-amidino transferase deficiency.
18
19 *Anal. Biochem.*, 343, 356–358.
20
21
22
23 61. Ippolito, D. M. and Eroglu, C. (2010) Quantifying synapses: an immunocytochemistry-based
24
25 assay to quantify synapse number. *J. Vis. Exp.*, 10.3791/2270.
26
27
28
29
30
31

32 Legends to figures

33
34 **Figure 1. Early deficiency of working memory in CrT^{-y} mice.** (a) Schematic diagram of the Y
35
36 maze apparatus. The mean number of entries in the single arms of the maze (A, B, C) and the total
37
38 number of arm entries were comparable for the different experimental groups (Two-Way ANOVA
39
40 on rank transformed data, post hoc Holm-Sidak method, $p = 0.506$, $p = 0.941$, $p = 0.276$, $p = 0.391$
41
42 respectively). (b) Alternation rate in the Y maze was significantly lower in CrT^{-y} mice ($n = 9$)
43
44 compared to that recorded for CrT^{+y} littermates ($n = 11$; t test, $p < 0.05$) at P28. * $p < 0.05$. Error
45
46 bars, s.e.m.
47
48
49
50
51

52 **Figure 2. Progressive impairment of object recognition memory in CrT^{-y} mice.** Top, a
53
54 schematic representation of the object recognition task. Histograms display object discrimination
55
56 indexes of CrT^{+y} and CrT^{-y} during the testing phase performed after a delay of 1 and 24h since the
57
58 sample phase at different ages. (a) P40. While both experimental groups can recognize the new
59
60

1
2
3 object in the test at 1h (t-test, $p = 0.285$), a significantly lower discrimination index was found in
4
5 $CrT^{-/y}$ mice ($n = 9$) compared to $CrT^{+/y}$ animals ($n = 7$; t-test, $p < 0.05$). (b) P100. Even if still not
6
7 significant, the recall capacity of $CrT^{-/y}$ animals at 1h was reduced (t test, $p = 0.242$). At 24h, a t-
8
9 test revealed that the performance of $CrT^{-/y}$ animals ($n = 11$) was strongly impaired with respect to
10
11 controls ($n = 10$; $p < 0.01$). (c) P180. A significant deficit of both short (t-test, $p < 0.05$) and long-
12
13 term (t-test, $p < 0.05$) memory was detected in mutant mice ($n = 10$) compared to controls ($n = 9$). *
14
15 $p < 0.05$; ** $p < 0.01$. Error bars, s.e.m.

16
17
18
19
20
21 **Figure 3. CrT deletion progressively deteriorates spatial learning and memory in mutant**

22 **mice.** (a) Left, learning curves for $CrT^{+/y}$ ($n = 10$, white) and $CrT^{-/y}$ mice ($n = 12$, grey) at P40. A
23
24 significant difference was detected at day 5 (Two way RM ANOVA, post hoc Holm-Sidak method,
25
26 $p < 0.05$). Right, histograms showing the mean swimming path covered to locate the submerged
27
28 platform on the last three days of training for the two groups. A significant difference between $CrT^{-/y}$
29
30 and $CrT^{+/y}$ animals was present (t-test, $p < 0.01$). Representative examples of swimming path
31
32 during the day 3 of the training phase for a $CrT^{+/y}$ (top) and a $CrT^{-/y}$ mouse (bottom) are also
33
34 reported. (b) Left, learning curves for $CrT^{+/y}$ ($n = 7$, white) and $CrT^{-/y}$ mice ($n = 8$, grey) at P100. A
35
36 significant difference was detected at day 5 (Two way RM ANOVA, post hoc Holm-Sidak method,
37
38 $p < 0.05$). Right, histograms showing the mean swimming path on the last three training days for
39
40 the two groups. A significant difference between $CrT^{+/y}$ and $CrT^{-/y}$ animals was present (t-test, $p <$
41
42 0.05). Representative examples of swimming path during the day 3 of the training phase for a
43
44 $CrT^{+/y}$ (top) and a $CrT^{-/y}$ mouse (bottom) are also reported. (c) Left, learning curves for $CrT^{+/y}$ ($n =$
45
46 9 , white) and $CrT^{-/y}$ mice ($n = 7$, grey) at P180: mutant mice were poorer learners with respect to
47
48 control littermates and a significant difference was detected at day 3, 4, 5 and 6 (Two way RM
49
50 ANOVA on rank transformed data, post hoc Holm-Sidak method, $p < 0.05$ for day 3 and 6, $p < 0.01$
51
52 for day 4 and 5). Right, histograms showing the mean swimming path on the last three day of
53
54 training. A t-test analysis showed a statistical difference between $CrT^{+/y}$ and $CrT^{-/y}$ animals ($p <$
55
56
57
58
59
60

0.01). Representative examples of swimming path during the day 3 of the training phase for a CrT^{+/y} (top) and a CrT^{-/y} mouse (bottom) are also depicted. * $p < 0.05$; # < 0.01 . Error bars, s.e.m.

Figure 4. CrT mutation enhance repetitive and stereotyped behaviors. (a) Social interaction behaviors in CrT^{-/y} mice. Histograms display discrimination indexes of CrT^{+/y} ($n = 6$) and CrT^{-/y} ($n = 8$) mice during the social preference (session I) and the social novelty phase (session II). No difference was detected between the two groups (Mann-Whitney Rank Sum test, $p = 0.662$ for session I; t-test, $p = 0.784$ for session II). A schematic representation of the three-chamber test is also depicted. (b) Performance of littermate wild-type ($n = 11$) and CrT^{-/y} mice ($n = 9$) on the accelerating rotarod. Inset shows an illustration of the rotarod apparatus. A Two Way ANOVA showed a significant effect of genotype ($p < 0.001$). Post hoc Holm-Sidak test revealed that the fall latency of mutant animals was significantly different from that of wild-type mice at all ages tested ($p < 0.01$ at P40 and P100, $p < 0.05$ at P180). A schematic representation of the rotarod test is also depicted. (c) Histograms display mean time spent self-grooming in CrT^{+/y} and CrT^{-/y} animals at P40 and P180. While no difference was detected at P40 (CrT^{+/y}, $n = 7$; CrT^{-/y}, $n = 9$; Two Way ANOVA on rank transformed data, post hoc Holm Sidak method, $p = 0.912$), CrT null mice exhibit increased grooming behavior at P180 (CrT^{+/y}, $n = 11$; CrT^{-/y}, $n = 7$; $p < 0.01$). A schematic representation of self-grooming behavior is reported. * $p < 0.05$; # < 0.01 . Error bars, s.e.m.

Figure 5. Synaptic neurotransmission in CrT^{+/y} and CrT^{-/y} animals at P180. (a) Left, representative immunostaining for vGlut1 from PFC and ACC of a CrT^{+/y} and a CrT^{-/y} mouse. Right, no difference in vGlut1 staining was detected between the two experimental groups ($n = 6$ for both groups) either in PFC (t-test, $p = 0.792$) or ACC (t-test, $p = 0.340$). (b) Left, representative immunostaining for vGAT from PFC and ACC of a CrT^{+/y} and a CrT^{-/y} mouse. The number of vGAT-positive puncta was significantly reduced both in the PFC and the ACC of mutant animals (n

1
2
3 = 9) with respect to controls (n = 8; t-test, p < 0.05 for both comparisons). * p < 0.05. Calibration
4
5 bars: 25 μ m. Error bars, s.e.m.
6
7

8
9
10 **Figure 6. Pathological activation of microglial cells in CrT^{-y} animals** (a) Left, representative
11 immunostaining for Iba1 from prefrontal cortex (PFC) of a CrT^{+y} and a CrT^{-y} mouse. Right, a
12 significant increase of the percentage of activated microglial cells, with a parallel decrease of
13 resting microglia, was detected in mutant mice with respect to wild-type animals (n = 8 for both
14 groups; Two Way ANOVA, post hoc Holm Sidak method, p < 0.01). (b) Left, representative
15 immunostaining for Iba1 from the hippocampus (HP) of a CrT^{+y} and a CrT^{-y} mouse. Right, the
16 percentage of activated microglia was increased in mutant mice, whereas the relative number of
17 resting cells was reduced compared to controls (n = 8 for both groups; Two Way ANOVA, post hoc
18 Holm Sidak method, p < 0.05). * p < 0.05; ** p < 0.01. Calibration bar: 100 μ m. Error bars, s.e.m.
19
20
21
22
23
24
25
26
27
28
29
30
31

32 **Figure 7. Neurogenesis impairment and enhanced lipofuscin accumulation in the**
33 **hippocampus of CrT^{-y} animals at P180.** (a) The hippocampal volume of CrT^{-y} mice was smaller
34 compared to CrT^{+y} mice (n = 6 for both groups; t-test, p < 0.05). (b) Stereological counting
35 revealed that the density of Ki67-positive cells was significantly reduced in the DG of CrT^{-y} mice,
36 with approximately 30% reduction with respect to wild-type littermates (n = 6 for both groups; t-
37 test, p < 0.01). (c) A significant decrease of the DCX-positive immature neurons was detected in the
38 hippocampus of adult CrT^{-y} mice compared to controls (n = 6 for both groups; t-test, p < 0.001). (d)
39 Representative immunostaining for Ki-67, a nuclear protein required for cellular proliferation, from
40 a CrT^{+y} and a CrT^{-y} mouse. (e) Representative immunostaining for DCX, a microtubule-associated
41 phosphoprotein expressed in early neuronal differentiation, from a CrT^{+y} and a CrT^{-y} mouse. (f)
42 Representative images for lipofuscin autofluorescence from a CrT^{+y} and a CrT^{-y} mouse. (g) Six-
43 month-old CrT^{-y} mice (n = 6) show extensive accumulation of autofluorescent material throughout
44 the brain when compared to the wild-type control (n = 5). A significant increase of abnormal
45
46
47
48
49
50
51
52
53
54
55
56
57
58
59
60

1
2
3 autofluorescent storage was mainly found in DG granular and polymorph layer of CrT^{-/-y} mice (t-
4 test, $p < 0.05$). * $p < 0.05$; ** $p < 0.01$; *** $p < 0.001$. Calibration bars: 50 μm . Error bars, s.e.m.
5
6
7
8

9 **Figure 8. A selective brain deletion of CrT is sufficient to impair cognitive functions and**
10 **hippocampal neurogenesis.** (a) Histograms display object discrimination indexes of nes-CrT^{+/-y}
11 and nes-CrT^{-/-y} during the testing phase performed after a delay of 1 and 24h since the sample phase
12 at P180. A significant deficit of both short (t-test, $p < 0.05$) and long-term (t-test, $p < 0.05$) memory
13 was detected in mutant mice ($n = 6$) compared to controls ($n = 8$). (b) Alternation rate in the Y maze
14 was significantly lower in nes-CrT^{-/-y} mice ($n = 6$) compared to that recorded for nes-CrT^{+/-y}
15 littermates ($n = 9$; t test, $p < 0.05$) at P180. (c) A significant decrease of the Ki67-positive cells was
16 detected in the hippocampus of P180 nes-CrT^{-/-y} mice compared to age-matched controls ($n = 6$ for
17 both groups; t-test, $p < 0.05$). * $p < 0.05$. Error bars, s.e.m.
18
19
20
21
22
23
24
25
26
27
28
29
30
31
32
33
34
35
36
37
38
39
40
41
42
43
44
45
46
47
48
49
50
51
52
53
54
55
56
57
58
59
60

Tissue (nmol/mg protein)	P30		P180	
	CrT ^{+/y}	CrT ^{-/y}	CrT ^{+/y}	CrT ^{-/y}
Cerebral cortex	76.36 ± 3.16	13.61 ± 1.06***	92.41 ± 0.66	14.15 ± 0.66***
Hippocampus	83.69 ± 4.37	14.14 ± 1.52***	88.73 ± 4.97	14.79 ± 1.46***
Muscle	310.20 ± 31.59	111.57 ± 21.27***	365.38 ± 8.19	15.94 ± 5.55***
Heart	89.92 ± 5.15	1.19 ± 0.27***	100.91 ± 3.36	2.39 ± 0.61***
Kidney	9.60 ± 0.65	1.59 ± 0.13*	10.36 ± 0.80	1.80 ± 0.78**

Table 1. Cr levels (mean ± SEM) in CrT^{+/y} and CrT^{-/y} animals at P30 and P180 (n = 4 per tissue for both groups). Cr levels have been measured by GC/MS. A reduction of Cr content was evident in the brain, muscle, heart and kidney of mutant animals at both P30 and P180 (Two Way ANOVA on rank transformed data, post hoc Holm-Sidak method). * p < 0.05; ** p < 0.01; *** p < 0.001.

Tissue (nmol/mg protein)	P30		P180	
	CrT ^{+/y}	CrT ^{-/y}	CrT ^{+/y}	CrT ^{-/y}
Cerebral cortex	0.060 ± 0.002	0.114 ± 0.016***	0.050 ± 0.006	0.066 ± 0.005
Hippocampus	0	0.091 ± 0.007 ***	0.026 ± 0.015	0.079 ± 0.009**
Muscle	0.106 ± 0.006	0.282 ± 0.068**	0.026 ± 0.010	0.150 ± 0.050**
Heart	0.094 ± 0.010	0.060 ± 0.004***	0.052 ± 0.007	0.033 ± 0.015
Kidney	10.700 ± 0.627	9.758 ± 0.712	2.205 ± 0.259	2.411 ± 0.112

Table 2. GAA levels (mean ± SEM) in CrT^{+/y} and CrT^{-/y} animals at P30 and P180 (n = 4 per tissue for both groups). At P30, a moderate increase of GAA content was evident in the brain and the muscle of mutant animals (Two Way ANOVA on rank transformed data, post hoc Holm-Sidak method, p < 0.05), whereas GAA was decreased in the heart of CrT^{-/y} animals (p < 0.05) and no difference was detected in the kidney tissue (p = 0.359). At P180, GAA levels were higher in the hippocampus and the muscle of mutant animals (Two Way ANOVA on rank transformed data, post hoc Holm-Sidak method, p < 0.01), whereas no difference was detected in cortex, heart and kidney (p = 0.175, p = 0.320 and p = 0.920, respectively). ** p < 0.01; *** p < 0.001.

Tissue (nmol/mg protein)	nes-CrT ^{+/y}	nes-CrT ^{-/y}	CrT ^{fl/y}
Cerebral cortex	73.29 ± 1.88	17.36 ± 0.87***	71.55 ± 4.15
Hippocampus	87.45 ± 4.17	17.13 ± 2.22 ***	94.62 ± 4.35
Muscle	382.97 ± 20.46	390.58 ± 22.66	385.36 ± 27.59
Heart	78.24 ± 3.72	70.35 ± 3.10	68.02 ± 1.79
Kidney	6.10 ± 0.81	3.11 ± 0.27	7.60 ± 1.22

Table 3. Cr levels (mean ± SEM) in nes-CrT^{+/y}, nes-CrT^{-/y} and CrT^{fl/y} animals at P180 (n = 4 per tissue for all groups). A reduction of Cr content was evident in the brain of mutant animals, while peripheral tissues were not affected (Two Way ANOVA on rank transformed data, post hoc Holm-Sidak method). * p < 0.001.**

Tissue (nmol/mg protein)	nes-CrT ^{+/y}	nes-CrT ^{-/y}	CrT ^{fl/y}
Cerebral cortex	0.048 ± 0.005	0.059 ± 0.004***	0.048 ± 0.004
Hippocampus	0.068 ± 0.005	0.131 ± 0.018*	0.074 ± 0.011
Muscle	0.054 ± 0.006	0.061 ± 0.002	0.059 ± 0.003
Heart	0.045 ± 0.004	0.047 ± 0.003	0.054 ± 0.007
Kidney	1.705 ± 0.373	1.231 ± 0.099	3.051 ± 0.914

Table 4. GAA levels (mean ± SEM) in nes-CrT^{+/y}, nes-CrT^{-/y} and CrT^{fl/y} animals at P180 (n = 4 per tissue for all groups). An increase of GAA content was evident in the brain of mutant animals, while peripheral tissues were not affected (Two Way ANOVA on rank transformed data, post hoc Holm-Sidak method). * p < 0.05; * p < 0.001.**

1
2
3
4
5
6
7
8
9
10
11
12
13
14
15
16
17
18
19
20
21
22
23
24
25
26
27
28
29
30
31
32
33
34
35
36
37
38
39
40
41
42
43
44
45
46
47
48
49
50
51
52
53
54
55
56
57
58
59
60**Point to point response letter to the Reviewers' comments:**

In the revised version of the manuscript, corrections to the former manuscript have been highlighted in yellow to simplify the reviewing process.

Response to Reviewer #1: (reviewer's comments are in italics)

This is a very well designed study in a creatine transporter deficient mouse model demonstrating a variety of cognitive and behavioral abnormalities in the knock-out model. Most importantly the study points to early brain aging associated with creatine depletion. The manuscript is well written and the conclusions are reasonable. Would be nice to have a bit more of a discussion about the fact that younger mice are not as creatine depleted in the muscle as compared to older age (P180).

We discussed the difference in muscular Cr levels between young (P30) and adult (P180) mice (p. 15). We detected a significant reduction of Cr levels in P180 CrT^{-/-} mice with respect to P30 CrT null mice only at level of muscular tissue, indicating that the compensatory upregulation of Cr biosynthesis in the muscle declines with age. Despite the ubiquitous pattern of CrT deletion, only few CCDS1 patients displayed an alteration of muscular Cr levels and strength (Puusepp et al., 2010). Our results raise the possibility that a muscular phenotype could occur also in patients later in life.

Also adding the guanidinoacetate concentrations to the table (why is this a figure 5?) would be helpful, instead of putting it in the supplement.

We included the results about guanidinoacetate levels in the main body of the manuscript (Table 2), as suggested by the reviewer. Figure 5 is now Table 1.

1
2
3 *BTW, the mouse chow (4RF21 GFP, Mucedola) is composed of 3.5% animal protein; therefore it is*
4
5 *NOT a creatine free chow. The statement 'the chow was not added with Cr (personal*
6
7 *communication of the manufacturer) (P17, l 13) is misleading.*
8
9

10
11
12 We removed the misleading sentence as suggested by the reviewer.
13
14
15

16 17 **Response to Reviewer #2:**

18
19 *The creatine transporter (CrT) deficiency is an X-linked inherited neurometabolic disorder*
20
21 *characterized by severe intellectual disability, epilepsy and autistic behaviors. The syndrome,*
22
23 *caused by mutations in SLC6A8, the creatine transporter 1 protein gene, is currently untreatable*
24
25 *due to the fact that creatine cannot pass the blood barrier. Very little is known on how deficiency in*
26
27 *brain creatine affects the development of neuronal circuits and their function in adulthood. In the*
28
29 *present manuscript, Baroncelli and colleagues provided significant novel data pointing to*
30
31 *important insights in the cellular and molecular mechanisms underlying the progression of the*
32
33 *disorder in the CrT mutant mice. The authors performed a longitudinal evaluation of cognitive*
34
35 *functions in CrT deficient mice and analyzed aging-related markers including synaptic number,*
36
37 *neuronal degeneration, hippocampal neurogenesis and neuroinflammation. They found a*
38
39 *progressive worsening of cognition as evaluated by novel object recognition, Y maze and Morris*
40
41 *Water Maze starting as early as postnatal day 28 until P180. At the cellular level, the authors*
42
43 *revealed a significant reduction of vGAT but not vGlut1 positive synapses across cortical layers*
44
45 *suggesting compromised inhibitory circuits. This was also accompanied by increased activated*
46
47 *microglia as indicated by iba-1 elevated expression, accumulation of autofluorescent lipofuscin*
48
49 *mainly in the dentate gyrus of hippocampus and reduced neurogenesis. The authors concluded that*
50
51 *loss of creatine induces precocious aging of neuronal circuits and progressive worsening of*
52
53 *cognitive performances.*
54
55
56
57
58
59
60

1
2
3 *The manuscript is well written, organized and the experiments are well executed with a significant*
4 *number of animals in each group and proper statistical analysis performed. The results are novel*
5 *and relevant.*
6
7
8
9

10
11
12 *There are only few points that the authors should address before the manuscript is suitable for*
13 *publication in Human Molecular Genetics.*
14

15
16
17 *1) It is important to keep in mind that in humans, the CNS is the main organ affected by creatine*
18 *deficiency syndrome. Indeed patients appear to have normal cardiac function and normal creatine*
19 *levels in the muscles. This is different from what the authors report here in the mouse model.*
20
21
22 *Therefore, it is important to understand whether a selective deletion of CrT in neuron would be*
23 *sufficient to recapitulate the cognitive and cellular defects described in the global deletion model.*
24
25
26 *The authors do not need to repeat the complete set of experiments performed in the total KO.*
27
28
29 *Rather they could focus in adulthood and perform cognitive behavioral evaluation together with*
30 *analysis of GABA circuits, microglia activation accumulation of lipofuscin.*
31
32
33
34
35
36
37
38

39 We totally agree with the reviewer about the importance to understand whether a selective deletion
40 of CrT in the central nervous system could be sufficient to recapitulate the phenotype displayed by
41 the ubiquitary knock-out model. Indeed, we had already developed a mouse carrying a floxed
42 *Slc6a8* gene. To target CrT deletion to neuronal and glial precursors widespread in the nervous
43 system, we crossed the floxed *Slc6a8* mouse with the Nestin::Cre recombinase mouse Tg(Nes-
44 cre)1Kln mouse from Jackson (<http://jaxmice.jax.org/strain/003771.html>). The resulting neural
45 specific KO displayed a selective loss of Cr and a slight GAA upregulation in cortex and
46 hippocampus but normal Cr levels in the periphery (Table 3, 4). Our behavioral investigation
47 highlighted that mutant (nes-CrT^{-y}) animals showed an impaired performance in the object
48 recognition test and a lower alternation rate in the Y maze, demonstrating an impairment of both
49 declarative and working memory reminiscent of the deficit described in the ubiquitary model. We
50
51
52
53
54
55
56
57
58
59
60

1
2
3 also investigated whether selective CrT deficiency could affect hippocampal neurogenesis.
4
5 Stereological analysis revealed that the number of Ki67-positive cell was significantly lower in the
6
7 DG of nes-CrT^{-/y} animal at P180. These results prove that the lack of CrT protein exclusively
8
9 restricted to brain cells is sufficient to recapitulate the cognitive and cellular defects displayed by
10
11 global knock-out mice. We included this new set of data in the manuscript by adding a new
12
13 paragraph in the result section and by presenting Figure 8. We also included a new paragraph in the
14
15 method section describing generation and genotyping of conditional CrT^{-/y} animals, and we
16
17 discussed these new results.
18
19
20
21
22
23

24
25 *2) The immunohistochemistry analysis of synaptic markers, microglia activation, neurogenesis,*
26
27 *were all performed at P180. These are very important data, however still do not tell us whether*
28
29 *these defects precede or accompany the onset of behavioral defects the author found already in the*
30
31 *juvenile animals. At a minimum, the authors should repeat the analysis at younger ages (P28*
32
33 *and/or P40) and compare the results with P180. In addition to corroborate the conclusion of*
34
35 *premature aging in CrT mice, the authors should analyze older control mice (>one year).*
36
37
38
39
40

41 We agree with the reviewer that a comparative analysis of synaptic markers, microglia activation
42
43 and neurogenesis in young and adult animals would increase the knowledge about cellular defects
44
45 underlying the onset and progression of pathological behavioral phenotype of CrT null mice. At
46
47 present, however, we do not have samples from young animals in storage and the length of time
48
49 required to obtain a sufficient number of CrT^{-/y} and CrT^{+/y} for this analysis would considerably
50
51 exceed the deadline for manuscript revision. Future studies will need to check the developmental
52
53 profile of markers modifications. We acknowledged this point in the discussion.
54
55
56
57
58
59

60 To further corroborate the hypothesis of a premature cognitive decline in CrT null mice, we
compared the performance in the MWM of P180 CrT^{-/y} animals and one-year old wild-type mice.

1
2
3 The mean distance to locate the platform on the last three days of training and the probe test
4 revealed a similar memory impairment in these two experimental groups. We included this new set
5 of data in the manuscript by adding a new paragraph in the Result section and by presenting Figure
6
7
8
9
10 S5.

11
12
13
14
15 *Minor point:*

16
17 *1) The color scheme used (white= mutant; grey = wild type) and the scheme presentation (first*
18 *mutant then control) make difficult to understand the results presented. I suggest to switch to white*
19 *for WT and solid color for the mutant and switch the order of the data, plotting first the control and*
20 *then the CrT-/y.*
21
22
23
24
25
26
27
28

29 We changed the color scheme and the scheme presentation of figures as suggested by the reviewers.
30
31
32
33
34
35
36
37
38
39
40
41
42
43
44
45
46
47
48
49
50
51
52
53
54
55
56
57
58
59
60

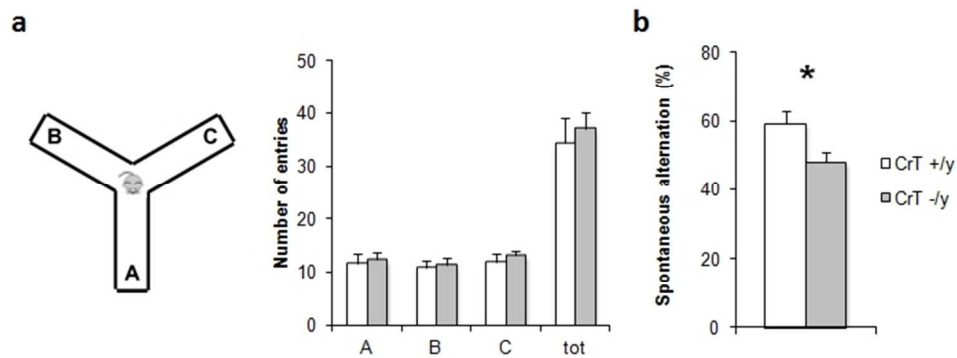
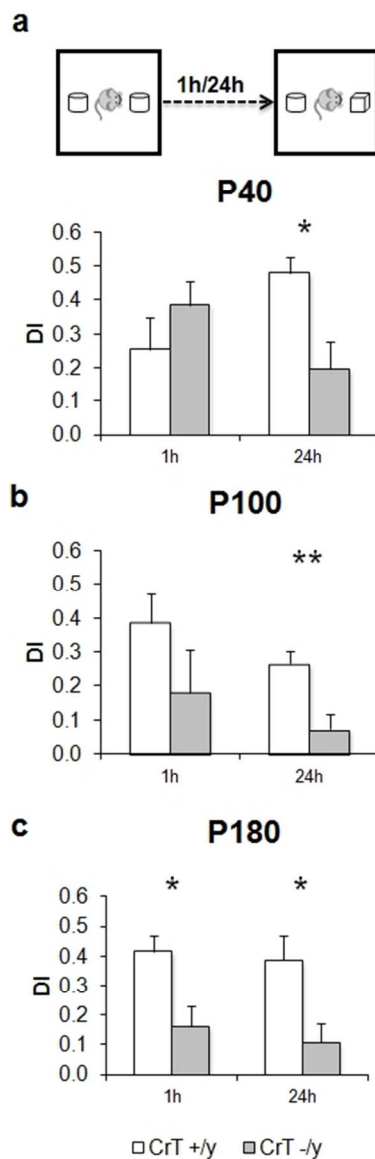


Figure 1. Early deficiency of working memory in CrT^{-/-} mice. (a) Schematic diagram of the Y maze apparatus. The mean number of entries in the single arms of the maze (A, B, C) and the total number of arm entries were comparable for the different experimental groups (Two-Way ANOVA on rank transformed data, post hoc Holm-Sidak method, $p = 0.506$, $p = 0.941$, $p = 0.276$, $p = 0.391$ respectively). (b) Alternation rate in the Y maze was significantly lower in CrT^{-/-} mice ($n = 9$) compared to that recorded for CrT^{+/y} littermates ($n = 11$; t test, $p < 0.05$) at P28. * $p < 0.05$. Error bars, s.e.m.



47
48
49
50
51
52
53
54
55
56
57
58
59
60

Figure 2. Progressive impairment of object recognition memory in CrT-/y mice. Top, a schematic representation of the object recognition task. Histograms display object discrimination indexes of CrT+/y and CrT-/y during the testing phase performed after a delay of 1 and 24h since the sample phase at different ages. (a) P40. While both experimental groups can recognize the new object in the test at 1h (t-test, $p = 0.285$), a significantly lower discrimination index was found in CrT-/y mice ($n = 9$) compared to CrT+/y animals ($n = 7$; t-test, $p < 0.05$). (b) P100. Even if still not significant, the recall capacity of CrT-/y animals at 1h was reduced (t test, $p = 0.242$). At 24h, a t-test revealed that the performance of CrT-/y animals ($n = 11$) was strongly impaired with respect to controls ($n = 10$; $p < 0.01$). (c) P180. A significant deficit of both short (t-test, $p < 0.05$) and long-term (t-test, $p < 0.05$) memory was detected in mutant mice ($n = 10$) compared to controls ($n = 9$). * $p < 0.05$; ** $p < 0.01$. Error bars, s.e.m.

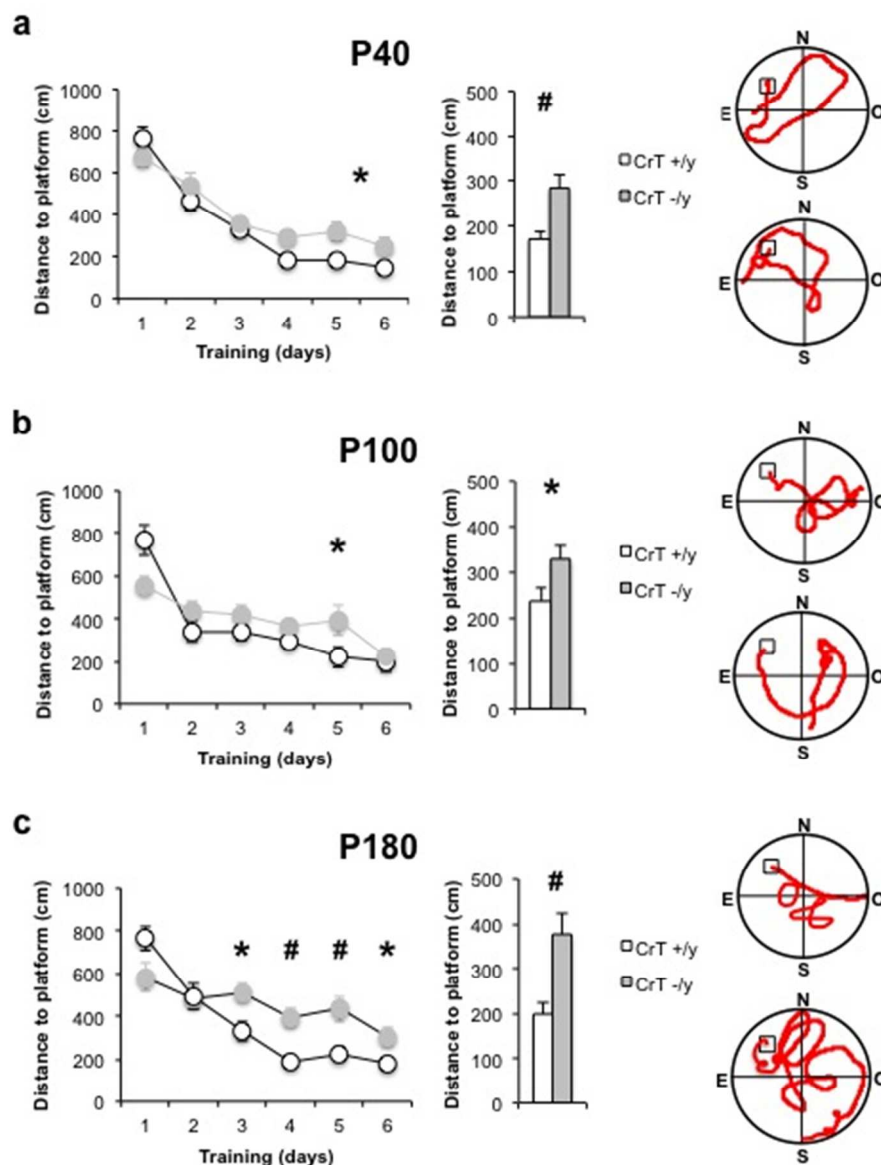


Figure 3. CrT deletion progressively deteriorates spatial learning and memory in mutant mice. (a) Left, learning curves for CrT+/y (n = 10, white) and CrT-/y mice (n = 12, grey) at P40. A significant difference was detected at day 5 (Two way RM ANOVA, post hoc Holm-Sidak method, $p < 0.05$). Right, histograms showing the mean swimming path covered to locate the submerged platform on the last three days of training for the two groups. A significant difference between CrT-/y and CrT+/y animals was present (t-test, $p < 0.01$). Representative examples of swimming path during the day 3 of the training phase for a CrT+/y (top) and a CrT-/y mouse (bottom) are also reported. (b) Left, learning curves for CrT+/y (n = 7, white) and CrT-/y mice (n = 8, grey) at P100. A significant difference was detected at day 5 (Two way RM ANOVA, post hoc Holm-Sidak method, $p < 0.05$). Right, histograms showing the mean swimming path on the last three training days for the two groups. A significant difference between CrT+/y and CrT-/y animals was present (t-test, $p < 0.05$). Representative examples of swimming path during the day 3 of the training phase for a CrT+/y (top) and a CrT-/y mouse (bottom) are also reported. (c) Left, learning curves for CrT+/y (n = 9, white) and CrT-/y mice (n = 7, grey) at P180: mutant mice were poorer learners with

1
2
3 respect to control littermates and a significant difference was detected at day 3, 4, 5 and 6 (Two way RM
4 ANOVA on rank transformed data, post hoc Holm-Sidak method, $p < 0.05$ for day 3 and 6, $p < 0.01$ for day
5 4 and 5). Right, histograms showing the mean swimming path on the last three day of training. A t-test
6 analysis showed a statistical difference between CrT+/y and CrT-/y animals ($p < 0.01$). Representative
7 examples of swimming path during the day 3 of the training phase for a CrT+/y (top) and a CrT-/y mouse
8 (bottom) are also depicted. * $p < 0.05$; # $p < 0.01$. Error bars, s.e.m.

9
10 167x222mm (72 x 72 DPI)

11
12
13
14
15
16
17
18
19
20
21
22
23
24
25
26
27
28
29
30
31
32
33
34
35
36
37
38
39
40
41
42
43
44
45
46
47
48
49
50
51
52
53
54
55
56
57
58
59
60

For Peer Review

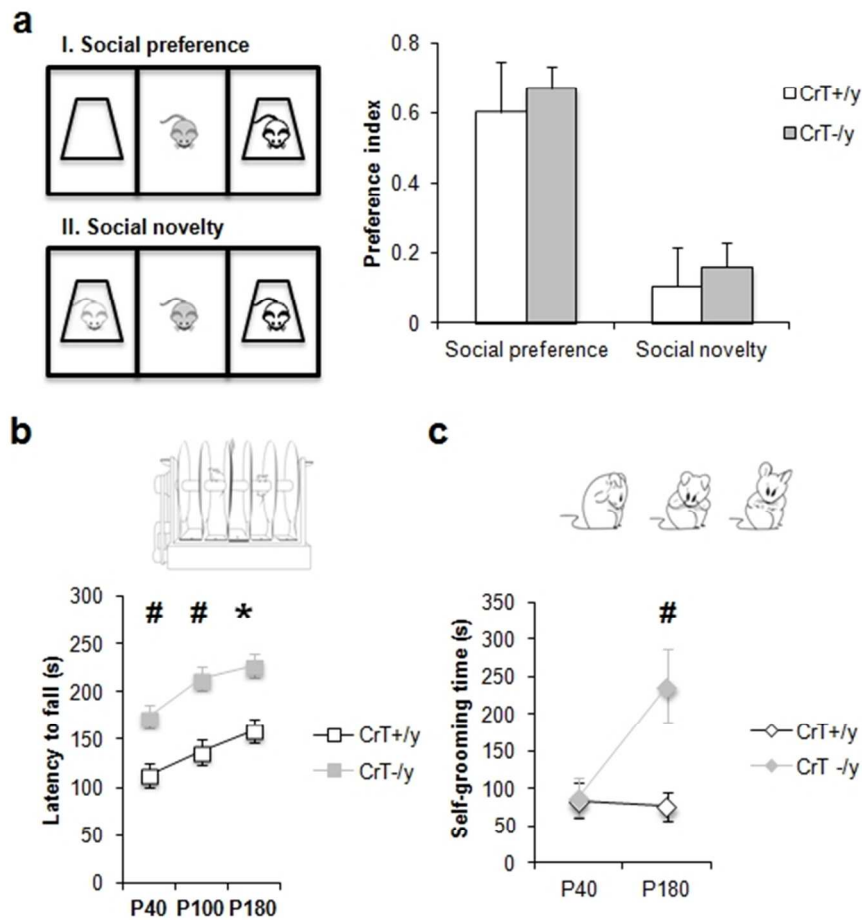


Figure 4. CrT mutation enhance repetitive and stereotyped behaviors. (a) Social interaction behaviors in CrT^{-/y} mice. Histograms display discrimination indexes of CrT^{+/y} (n = 6) and CrT^{-/y} (n = 8) mice during the social preference (session I) and the social novelty phase (session II). No difference was detected between the two groups (Mann-Whitney Rank Sum test, p = 0.662 for session I; t-test, p = 0.784 for session II). A schematic representation of the three-chamber test is also depicted. (b) Performance of littermate wild-type (n = 11) and CrT^{-/y} mice (n = 9) on the accelerating rotarod. Inset shows an illustration of the rotarod apparatus. A Two Way ANOVA showed a significant effect of genotype (p < 0.001). Post hoc Holm-Sidak test revealed that the fall latency of mutant animals was significantly different from that of wild-type mice at all ages tested (p < 0.01 at P40 and P100, p < 0.05 at P180). A schematic representation of the rotarod test is also depicted. (c) Histograms display mean time spent self-grooming in CrT^{+/y} and CrT^{-/y} animals at P40 and P180. While no difference was detected at P40 (CrT^{+/y}, n = 7; CrT^{-/y}, n = 9; Two Way ANOVA on rank transformed data, post hoc Holm Sidak method, p = 0.912), CrT null mice exhibit increased grooming behavior at P180 (CrT^{+/y}, n = 11; CrT^{-/y}, n = 7; p < 0.01). A schematic representation of self-grooming behavior is reported. * p < 0.05; # < 0.01. Error bars, s.e.m.

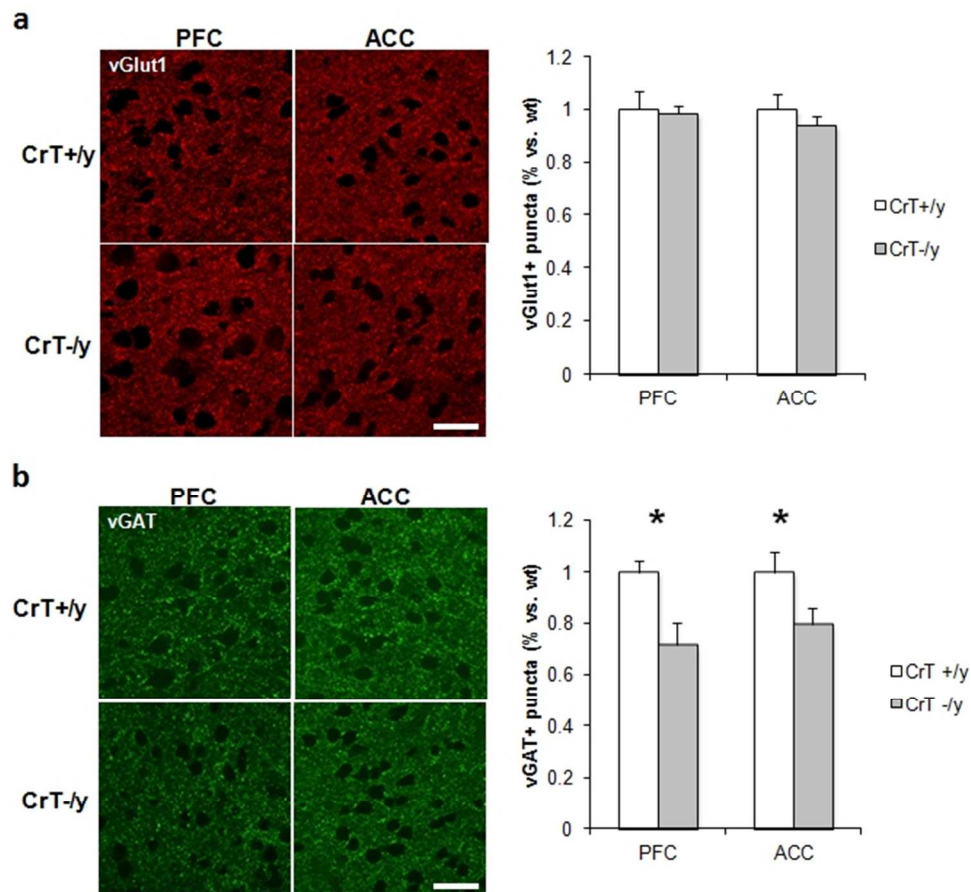
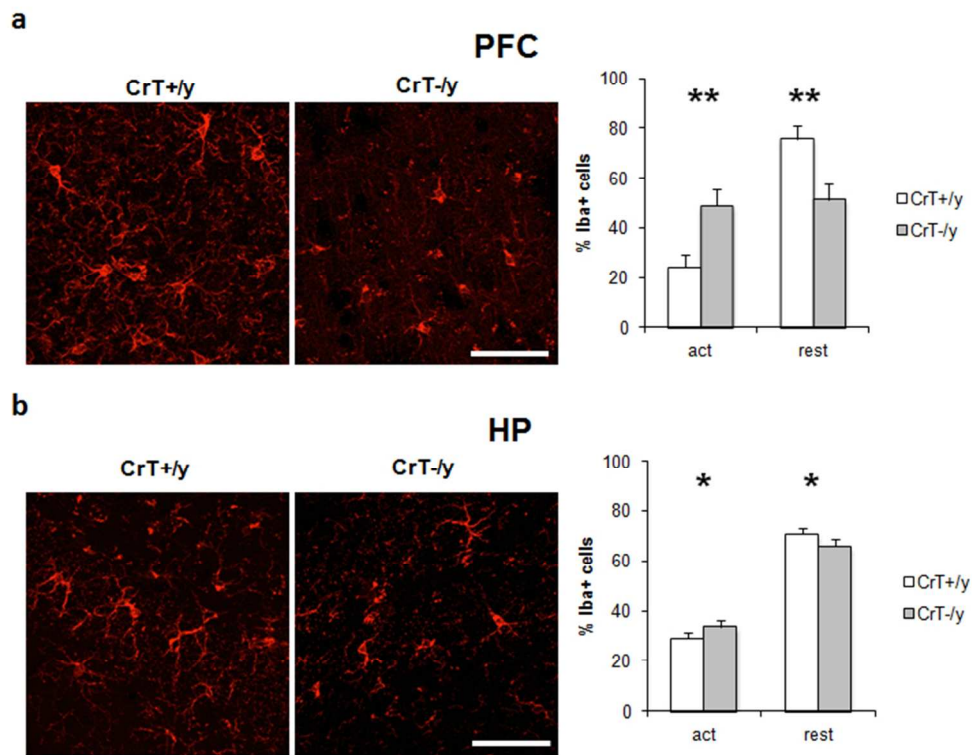


Figure 5. Synaptic neurotransmission in CrT+/y and CrT-/y animals at P180. (a) Left, representative immunostaining for vGlut1 from PFC and ACC of a CrT+/y and a CrT-/y mouse. Right, no difference in vGlut1 staining was detected between the two experimental groups ($n = 6$ for both groups) either in PFC (t-test, $p = 0.792$) or ACC (t-test, $p = 0.340$). (b) Left, representative immunostaining for vGAT from PFC and ACC of a CrT+/y and a CrT-/y mouse. The number of vGAT-positive puncta was significantly reduced both in the PFC and the ACC of mutant animals ($n = 9$) with respect to controls ($n = 8$; t-test, $p < 0.05$ for both comparisons). * $p < 0.05$. Calibration bars: 25 μm . Error bars, s.e.m.



33
34
35
36
37
38
39
40
41
42
43
44
45
46
47
48
49
50
51
52
53
54
55
56
57
58
59
60

Figure 6. Pathological activation of microglial cells in CrT⁻/y animals (a) Left, representative immunostaining for Iba1 from prefrontal cortex (PFC) of a CrT⁺/y and a CrT⁻/y mouse. Right, a significant increase of the percentage of activated microglial cells, with a parallel decrease of resting microglia, was detected in mutant mice with respect to wild-type animals (n = 8 for both groups; Two Way ANOVA, post hoc Holm Sidak method, p < 0.01). (b) Left, representative immunostaining for Iba1 from the hippocampus (HP) of a CrT⁺/y and a CrT⁻/y mouse. Right, the percentage of activated microglia was increased in mutant mice, whereas the relative number of resting cells was reduced compared to controls (n = 8 for both groups; Two Way ANOVA, post hoc Holm Sidak method, p < 0.05). * p < 0.05; ** p < 0.01. Calibration bar: 100 μm. Error bars, s.e.m.

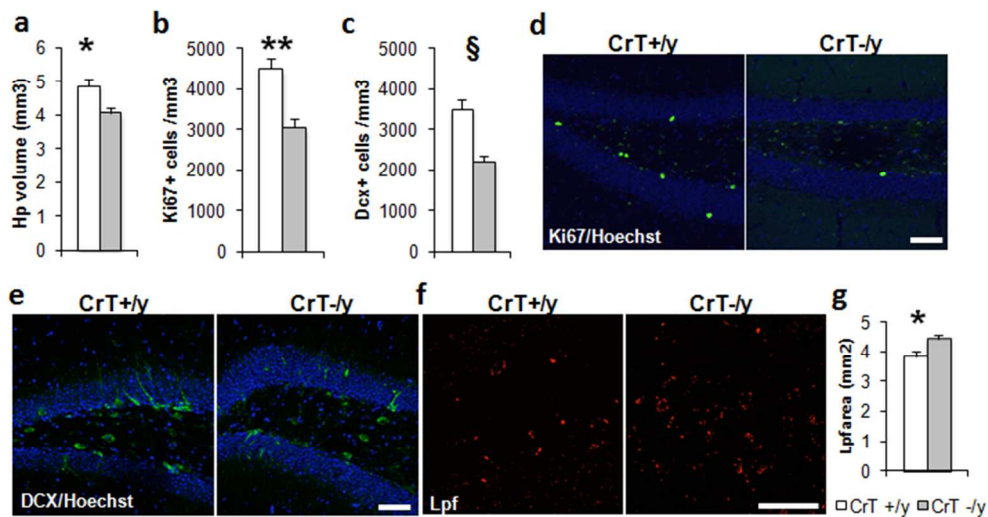


Figure 7. Neurogenesis impairment and enhanced lipofuscin accumulation in the hippocampus of CrT⁻/y animals at P180. (a) The hippocampal volume of CrT⁻/y mice was smaller compared to CrT⁺/y mice (n = 6 for both groups; t-test, p < 0.05). (b) Stereological counting revealed that the density of Ki67-positive cells was significantly reduced in the DG of CrT⁻/y mice, with approximately 30% reduction with respect to wild-type littermates (n = 6 for both groups; t-test, p < 0.01). (c) A significant decrease of the DCX-positive immature neurons was detected in the hippocampus of adult CrT⁻/y mice compared to controls (n = 6 for both groups; t-test, p < 0.001). (d) Representative immunostaining for Ki-67, a nuclear protein required for cellular proliferation, from a CrT⁺/y and a CrT⁻/y mouse. (e) Representative immunostaining for DCX, a microtubule-associated phosphoprotein expressed in early neuronal differentiation, from a CrT⁺/y and a CrT⁻/y mouse. (f) Representative images for lipofuscin autofluorescence from a CrT⁺/y and a CrT⁻/y mouse. (g) Six-month-old CrT⁻/y mice (n = 6) show extensive accumulation of autofluorescent material throughout the brain when compared to the wild-type control (n = 5). A significant increase of abnormal autofluorescent storage was mainly found in DG granular and polymorph layer of CrT⁻/y mice (t-test, p < 0.05). * p < 0.05; ** p < 0.01; *** p < 0.001. Calibration bars: 50 μ m. Error bars, s.e.m.

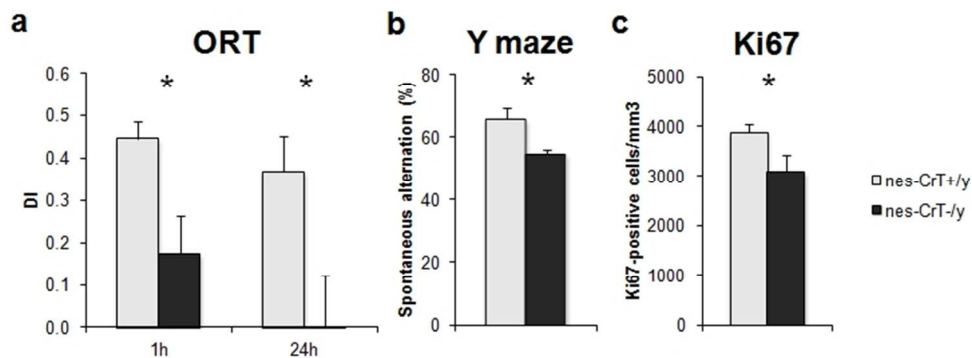


Figure 8. A selective brain deletion of CrT is sufficient to impair cognitive functions and hippocampal neurogenesis. (a) Histograms display object discrimination indexes of nes-CrT+/y and nes-CrT-/y during the testing phase performed after a delay of 1 and 24h since the sample phase at P180. A significant deficit of both short (t-test, $p < 0.05$) and long-term (t-test, $p < 0.05$) memory was detected in mutant mice ($n = 6$) compared to controls ($n = 8$). (b) Alternation rate in the Y maze was significantly lower in nes-CrT-/y mice ($n = 6$) compared to that recorded for nes-CrT+/y littermates ($n = 9$; t test, $p < 0.05$) at P180. (c) A significant decrease of the Ki67-positive cells was detected in the hippocampus of P180 nes-CrT-/y mice compared to age-matched controls ($n = 6$ for both groups; t-test, $p < 0.05$). * $p < 0.05$. Error bars, s.e.m.